5-2016

THE ROLE OF SKELETAL MUSCLE-SYNTHESIZED BRAIN-DERIVED NEUROTROPHIC FACTOR IN RETROGRADE TRANSPORT ALONG MOTORNEURON AXONS

Rebecca L. Dangremond
Northern Michigan University, rdangrem@nmu.edu

THE ROLE OF SKELETAL MUSCLE-SYNTHESIZED BRAIN-DERIVED
NEUROTROPHIC FACTOR IN RETROGRADE TRANSPORT ALONG
MOTORNEURON AXONS

By

Rebecca L. Dangremond

THESIS

Submitted to
Northern Michigan University
In partial fulfillment of the requirements
For the degree of

MASTER OF SCIENCE

Office of Graduate Education and Research

May 2016

SIGNATURE APPROVAL FORM

THE ROLE OF SKELETAL MUSCLE-SYNTHESIZED BRAIN-DERIVED
NEUROTROPHIC FACTOR IN RETROGRADE TRANSPORT ALONG
MOTORNEURON AXONS

This thesis by Rebecca L. Dangremond is recommended for approval by the student's
Thesis Committee and Department Head in the Department of Biology and by the
Assistant Provost of Graduate Education and Research.

_____
Committee Chair: Dr. Erich Ottem   Date

_____
Department Head and First Reader: Dr. John Rebers   Date

_____
Second Reader: Dr. Josh Sharp   Date

_____
Dr. Robert J. Winn   Date
Interim Assistant Provost of Graduate Education and Research

ABSTRACT

THE ROLE OF SKELETAL MUSCLE-SYNTHESIZED BRAIN-DERIVED
NEUROTROPHIC FACTOR IN RETROGRADE TRANSPORT ALONG
MOTORNEURON AXONS

By

Rebecca L. Dangremond

Brain-derived neurotrophic factor (BDNF) is a neurotrophic signaling protein

required for the development, maintenance and overall health and survival of neurons

(Greenberg et al., 2009; Lu et al., 2005; Reichardt, 2006). BDNF is synthesized in

several tissue types, including skeletal muscle (Matthews et al., 2009). Skeletal muscle-

BDNF binds to its cognate receptor, tyrosine receptor kinase B (TrkB), located on the

axon terminals of innervating motorneurons, initiating signaling cascades known to

promote the health, maintenance and survival of motorneurons (Lee et al., 2001). In

order for signaling to occur in the cell body, where transcription of survival genes occurs,

the TrkB-BDNF complex is endocytosed and transported via retrograde transport

mechanisms along the axon to the cell soma (Ginty and Segal, 2002). Disruptions of the

retrograde transport of neurofilament subunits, vesicular proteins, androgen receptor,

neurotrophin-Trk complexes, mitochondria and or other organelles are implicated in such

neurodegenerative diseases as Huntington's disease, Spinal Bulbar Muscular Atrophy,

Charcot-Marie Tooth Disease and Amyotrophic Lateral Sclerosis (Chevalier-Larsen et

al., 2006). Reduction of BDNF synthesis is a characteristic of these diseases as well

(Howells et al., 2000; Jiang et al., 2005; Liu et al., 2005). We hypothesized that skeletal

muscle-BDNF is required for normal retrograde transport of neurofilament-H, the

vesicular protein synaptophysin, and mitochondria in motorneuron axons. We used Cre-

Lox gene recombination technology to generate skeletal muscle-BDNF knockout animals. We first measured the accumulation of the retrogradely transported phosphorylated-neurofilament-H (NF-H-P) protein at distal axons in young (30 day old; 30d) and young-adult (120d) transgenic mice. We found that there is significant accumulation of this protein at this site in 120d skeletal muscle-synthesized BDNF deficient mice. Preliminary data show that there is no significant accumulation of NF-H-P in skeletal muscle-BDNF deficient mice at 30d. We next performed sciatic nerve ligation experiments in which the sciatic nerve of 30d and 120d mice was obstructed by a ligature. We found that 8 hours post-procedure there was significantly less accumulation of retrogradely transported NF-H-P and the motor associated protein, dynactin 1, immediately distal to the ligation site in skeletal muscle-BDNF deficient mice. While preliminary data for 30d animals show trends for increased accumulation of NF-H-P and synaptophysin in the distal ligation site, they do not reach significance. Together, these results indicate that loss of skeletal muscle-synthesized BDNF leads to disruptions in retrograde transport in 120d animals. Lastly, we investigated potential accumulation of mitochondria at the presynapse due to a decrease in retrograde transport of old and or damaged mitochondria being trafficked to the cell body for recycling. We injected the mitochondrial dye MitoTracker into the gastrocnemius muscle of 120d transgenic animals and measured the colocalization of this dye with presynaptic and postsynaptic immunofluorescent markers. Our results indicate that there is a significant decrease in mitochondria at the presynaptic terminal in 120d skeletal muscle-BDNF deficient mice.

AKNOWLEDGEMENTS

I would like to thank my advisor and mentor, Dr. Erich Ottem, for truly investing his time and energy into shaping me into the experienced and confident researcher I have become. I take comfort in knowing that my support from Erich will not end when the thesis paperwork has been signed, and that I will have it for the many years to come.

I appreciate Dr. John Rebers and Dr. Josh Sharp for agreeing to be on my committee and for their valuable input on this research. Thank you for kindly extending your knowledge and resources.

Thank you to my academic sister, Mandy Taisto, for all of the training, advice and friendship she bestowed upon me.

Thank you to all of the Ottem Lab members who have volunteered their time to help directly or indirectly with this project. Special thank you to Jenna Ennamany, Elizabeth O'Brien, Alison Bosink, Tiaira Porter and Carly Agee, for always going the extra mile, driven by a genuine interest in the work that we do.

I would like to thank the Dean of the College of Arts and Sciences, Michael Broadway, for securing the confocal microscope that made this research project possible.

I would like to thank Dr. Mary Etchison of NMU's Counseling and Consultation Services for helping me with my personal health and wellbeing during this project. I may not have succeeded without your talented efforts.

Thank you to my incredible family support system which includes, but is certainly not limited to, my parents: Carmen and Jeff Dangremond, my brothers: Eric and Matthew Dangremond, and my boyfriend: Zach Mueller.

This thesis follows formatting guidelines provided by the Department of Biology. References in this thesis are written in accordance with the guidelines for the journal *Cell*: http://www.cell.com/cell/authors.

TABLE OF CONTENTS

LIST OF FIGURES

LIST OF ABBREVIATIONS

ALS – amyotrophic lateral sclerosis
AMPK – 5' AMP-activated protein kinase
ANOVA – analysis of varience
AP2 – adaptor protein 2
AR – androgen receptor
ARP1 – actin-related protein 1
BAD – BCL-2 associated death protein
BC – bulbocavernosus
BDNF – brain derived neurotrophic factor
BTX-A – botulinum toxin type A
CREB – cyclicAMP response element binding protein
d – days old
DAG – diacylglycerol
DCTN1 – dynactin 1
Gastroc – gastrocnemius
HSA – human skeletal actin
HD – Huntington's disease
IC – intermediate chain
IP3 – inositol triphosphate
LA – levator ani
MAPK – mitogen activated protein kinase
MEK – MAPK/ERK kinase
NGF – nerve growth factor
NSAID – non steroidal anti inflammatory
NT-3 – neurotrophin-3
NT-4 – neurotrophin -4
p75NTR – p75 neurotrophic receptor
PI3K – phosphatidylinositol-3 kinase
PLCγ - phospholipase C gamma
sALS – sporadic ALS
SBMA- spinal and bulbar muscular atrophy
SMA – spinal muscular atrophy
SNB – spinal nucleus of the bulbocavernosus
Trk – tyrosine receptor kinase
UPS – ubiquitin-proteasome system
VAChT – vesicular acetyl choline transporter
Voxel – volumetric pixel

CHAPTER ONE: INTRODUCTION AND LITERATURE REVIEW

Neurons rely on neurotrophic proteins to support development, growth, survival,

plasticity and other cellular processes (Greenberg et al., 2009; Lu et al., 2005; Reichardt,

2006). Four well-known neurotrophins identified in mammals include nerve growth

factor (NGF), brain-derived neurotrophic factor (BDNF), neurotrophin-3 (NT-3) and

neurotrophin-4 (NT-4). Each neurotrophin has a precursor, or pro-neurotrophin. The

pro-neurotrophins have high affinity for the p75 neurotrophic receptor (p75NTR).

Mature neurotrophins bind to the tyrosine receptor kinase (Trk) class of receptors. Nerve

growth factor binds specifically to TrkA, BDNF and NT-4 bind to TrkB, and NT-3 binds

to TrkC. Pro-neurotrophins can be proteolytically cleaved intracellularly before secretion

or extracellularly after secretion. Alternatively, they can also be secreted as full-length

pro-neurotrophins without prior cleavage of regulatory domains (Lee et al., 2001).

BDNF is the most well-characterized neurotrophin due to the many and important roles it

has in maintaining normal functioning and survival of neurons in the mature nervous

system. For example, BDNF promotes long-term potentiation in synaptic spines while

also inhibiting long-term depression in neurons of the hippocampus and visual cortex (Lu

et al., 2005). Contrary to what its name may suggest, BDNF is synthesized in several

tissue types in addition to the brain, including thymus, heart, lung, skeletal muscle and

other tissues (Matthews et al., 2009). BDNF is most often secreted as proBDNF and is

proteolytically cleaved extracellularly before binding to TrkB (Mowla et al., 2001).

Once bound to its receptor, the mature BDNF-TrkB complex activates multiple

signaling cascades, including the phospholipase-Cγ (PLCγ), phosphatidylinositol-3

kinase (PI3K), and mitogen-activated protein kinase (MAPK)-MEK (MAPK/ERK kinase) signaling pathways (Dijkhuizen and Ghosh, 2005; Reichardt, 2006). Following activation, each pathway is responsible for maintaining normal cellular functions. PI3K maintains cell survival by activating Akt, which inhibits the apoptotic activities of BCL2-associated death protein (BAD) and forkhead (Brunet et al., 1999; Datta et al., 1997; del Peso et al., 1997). Generation of inositol triphosphate (IP_3) and diacylglycerol (DAG) via the activation of the PLCγ signaling pathway results in the mobilization of Ca^{2+} stores and subsequent activation of Ca^{2+}- and DAG-regulated protein kinases. Ultimately, this pathway leads to activation of ion channels and the expression of several transcription factors. The MAPK-MEK signaling cascade stimulates the activity of anti-apoptotic proteins including BCL-2 as well as the expression of transcription factors including cAMP response element binding protein (CREB). Phosphorylation of CREB via the MAP kinase cascade activates transcription of genes essential for normal differentiation and prolonged survival of neurons (Aloyz et al., 1998; Riccio et al., 1999). BDNF signaling induces axonal branching, dendritic growth, and increases synaptic spine density and number (Lu et al., 2005; Reichardt, 2006).

BDNF can act as both an anterograde and retrograde signaling protein. As an anterograde signaling protein, BDNF synthesized in the neural soma is subsequently transported down axonal microtubules and released from the presynaptic terminal to act on the cell which released BDNF (in an autocrine fashion) or on post-synaptic cells (Altar et al., 1997; Cheng et al., 2011). As a retrograde signaling protein, BDNF released from a postsynaptic cell can influence the activity of the presynaptic neuron (Ginty and Segal, 2002). At some active synapses, BDNF may be exocytosed by the postsynaptic cell and

bind to receptors expressed by the presynaptic neurons. Once bound, the BDNF-TrkB

complex is subsequently endocytosed and transported to the cell body via the molecular

motor dynein (Cosker and Segal, 2014; Howe and Mobley, 2005). Binding of BDNF to

TrkB initiates the PLCγ, PI3K and MAPK-MEK signaling pathways described above.

These three signal transduction pathways are thus activated at the cell terminal, along the

axon as the BDNF-TrkB signaling endosome is transported, and at the cell body where

the signaling endosome is delivered (Ginty and Segal, 2002). The retrograde transport of

BDNF-TrkB signaling endosomes is critical to the health of many neurons, as described

below.

The importance of BDNF is underscored by the pathologies associated with its

absence or reduction. While global BDNF knockout results in embryonic death, a

reduction in BDNF in specific neural subpopulations is a common characteristic of

neurodegenerative diseases including Parkinson's, Huntington's, amyotrophic lateral

sclerosis (ALS), spinal muscular atrophy (SMA) and spinal and bulbar muscular atrophy

(SBMA; Howells et al., 2000; Jiang et al., 2005; Liu et al., 2005). While BDNF

synthesized by neurons in the brain and spinal cord has been studied for several years,

our research group sought to investigate the less-understood role of BDNF that is

synthesized by skeletal muscle. Gazula et al., (2004) published one of the first studies to

demonstrate that some type of trophic signaling from skeletal muscles is important in the

maintenance of innervating motorneurons. In their experiments, rats underwent complete

spinal cord transection between T4 – T6, rendering their hind limbs paralyzed.

Transection followed by inactivity led to dramatic atrophy and loss of dendritic branching

of soleus-associated motorneurons. In contrast, rats that underwent forced hind-limb

exercise which activated local interneuron-regulated reflexes showed less pathology of

soleus-associated motorneurons when compared to sedentary transected rats. These

findings suggested that some diffusible factor of muscle-origin was communicating to the

denervated motorneurons and was alleviating dendritic atrophy.   There has since been

ample evidence that skeletal-muscle synthesized BDNF mediates this important signaling

role.

Gomez-Pinilla et al., (2002) performed experiments showing that voluntary

exercise leads to increased BDNF mRNA and protein in both the spinal cord and soleus

muscle. Spinal cords of male Sprague-Dawley rats that were housed with running wheels

for 7d showed increased BDNF mRNA and protein to compared to spinal cords of

sedentary counterparts who were not housed with running wheels. The authors noted a

direct relationship between the fold-increase in BDNF mRNA in the spinal cord and

distance ran by the rats. In the soleus, BDNF mRNA and protein were significantly

increased at day 7d as well. In another experiment, Gomez-Pinilla et al., injected

botulinum toxin type A (BTX-A) into the right soleus of male Sprague-Dawley rats,

rendering the muscle paralyzed. Sedentary animals showed a decrease in BDNF mRNA

in the BTX-A injected soleus and in the spinal cord ipsilateral to the BTX-A injected

muscle. After 7d of exercise, BDNF mRNA was increased in the contralateral spinal

cord, and decreased in the ipsilateral spinal cord relative to BDNF mRNA levels in

contralateral spinal cord of sedentary animals. Furthermore, after 7d of exercise BDNF

mRNA levels were increased in the non-injected soleus and decreased in the BTX-A-

injected soleus relative to the non-injected soleus of sedentary rats (Gómez-Pinilla et al.,

2002). Together these data provide evidence that voluntary exercise results in increased

BDNF synthesis in skeletal muscle and motorneurons.

In other studies, research involving the motorneurons of the spinal nucleus of the

bulbocavernosus (SNB) and their target muscles, the bulbocavernosus (BC) and levator

ani (LA) muscles, highlights the critical role muscle-synthesized BDNF plays in the

normal physiology of associated motorneurons (See Ottem et al., 2013 for review). It is

important to note that SNB motorneurons are dependent on androgens for survival during

development, but also depend on the steroids for the maintenance of morphological

integrity in adulthood. Lack of androgen in adulthood due to castration leads to somal

and dendritic atrophy in SNB motorneurons. Therefore, expression and synthesis of

androgen receptor (AR) is critical to the physiology and health of SNB motorneurons.

Experiments in which the SNB motorneurons are axotomized show that there is a

subsequent decrease in AR expression (Al-Shamma and Arnold, 1995; Kamal and

Goldstein, 2002; Yang and Arnold, 2000a) as well as cell body and dendritic atrophy

(Yang and Arnold, 2000b; Yang et al., 2004). Many of the atrophic effects in SNB

motorneurons are alleviated upon reinnervation of target muscles, indicating that the

BC/LA target muscles of SNB motorneurons are a source of regulatory factors

influencing AR expression and, ultimately, motorneuron morphology (Bisby and

Tetzlaff, 1992; Bodo and Rissman, 2008; Brännström et al., 1992; O'Hanlon and Lowrie,

1995; Sumner and Watson, 1971). To determine which BC/LA muscle-synthesized

neurotrophic factor(s) are involved in the regulation of AR in motorneurons of the SNB,

Al-Shamma and Arnold applied several neurotrophic factors to the axotomized stumps of

SNB motorneurons. They found that BDNF was the only neurotrophic factor that

reversed the atrophic effects of axotomy on SNB motorneurons, thus indicating the likelihood that the target skeletal muscle may be the origin of trophic factor that maintain the health and morphology of motorneurons (Al-Shamma and Arnold, 1997).

In current studies, we have generated a transgenic mouse model that enables us to further investigate the role of muscle-synthesized BDNF. Using cre-lox gene technology, described below, we generated mice that lack one or both copies of the BDNF gene in skeletal muscles specifically. Behaviorally, these animals display a phenotype similar to animal models of neuromuscular disease, including ALS and SBMA. Both the heterozygous and homozygous skeletal muscle-synthesized BDNF knockouts (Muscle$^{BDNF+/-}$ and Muscle$^{BDNF-/-}$, respectively) struggle to remain on a suspended rotating rod, have reduced grip strength and higher clasping scores compared to their wildtype (Muscle$^{BDNF+/+}$) counterparts. All of these behaviors are adult-onset. Following histological analysis, we found that there is significant muscle pathology in the gastrocnemius (gastroc) muscle, including both hypertrophic and hypotrophic fibers, fiber splitting, centralized nuclei, and an overall age-independent loss of fibers in heterozygous and homozygous knockouts at 30d, 90d, 120d, 180d and 210d (see Figures 1 and 2). We don't see such extensive myopathology when looking at the soleus. Only 30d homozygous knockouts have significantly greater myopathology compared to control animals (see Figures 3 and 4).
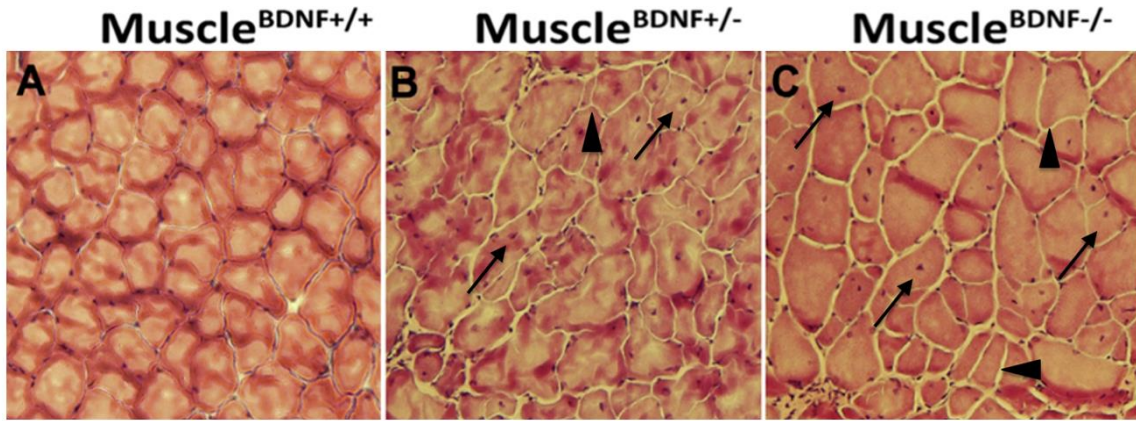
Figure 1. Muscle pathology in gastroc fibers of muscle synthesized-BDNF deficient 120d mice. Gastroc fibers of controls appear healthy with nuclei located at the periphery of the fibers and no fiber splitting is observed (A). Heterozygous and homozygous knockouts (B and C respectively) exhibit multiple centralized nuclei (arrows) and split fibers (arrowheads). Also note extensive hypertrophy and hypotrophy in homozygous knockouts (C). Taisto et al., 2013
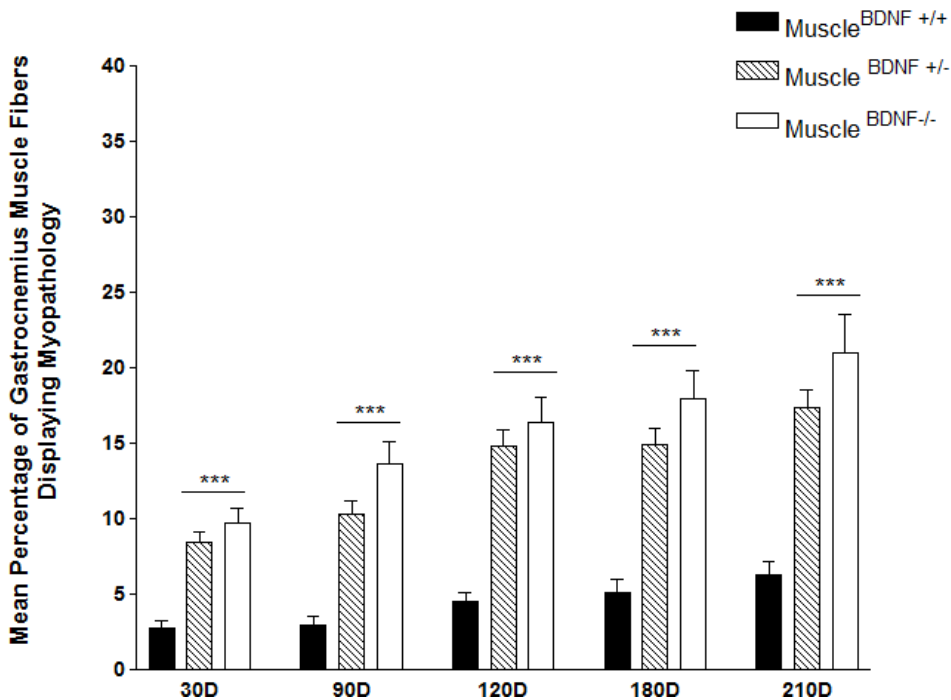
Figure 2. Mean percentage of gastroc muscle fibers displaying myopathology in control and experimental animals. Significant increases in myopathology are seen in both heterozygous and homozygous knockouts at all age groups compared to control animals.
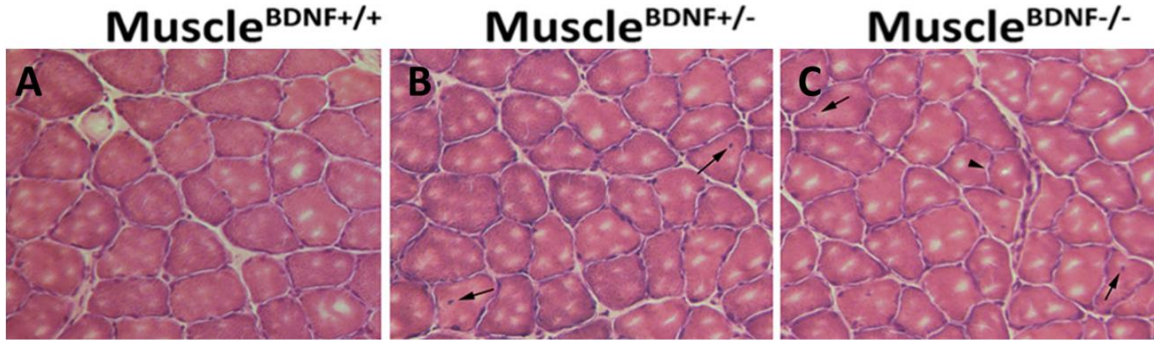
Figure 3. Muscle pathology in soleus fibers of muscle synthesized-BDNF deficient 120d mice. While control animal soleus fibers appear normal (A), heterozygous and homozygous knockout animals (B and C respectively) show some centralized nuclei (arrows) and fiber splitting (arrowhead).
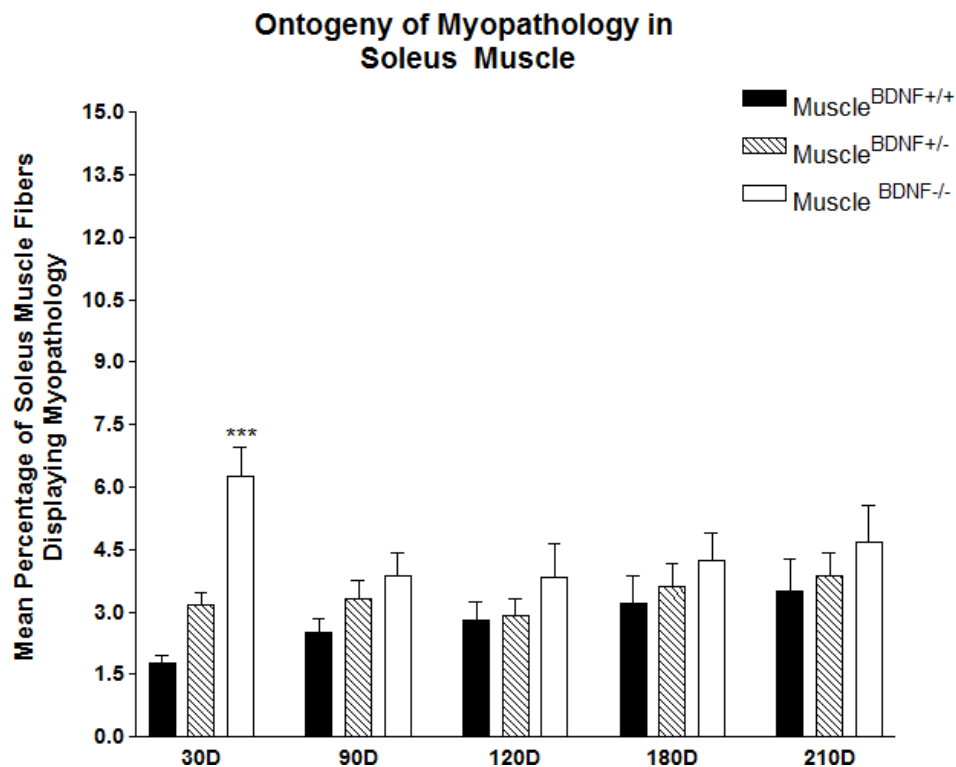
Figure 4. Mean percentage of soleus muscle fibers displaying myopathology in control and experimental animals. Only 30d homozygous knockout animals show significant increases in myopathology compared to controls. No significant changes are seen in heterozygous knockout animals at any time point, or in homozygous knockouts at 90d, 120d, 180d or 210d.

When assessing the surface area of the neuromuscular junction, we found that the presynapse, labeled with anti-vesicular acetylcholine transporter, is smaller in 120d homozygous knockout animals compared to control animals (see Figure 5A). There are no significant changes in postsynaptic surface area, labeled with α-bungarotoxin, across genotypes in 120d animals (see Figure 5B). When assessing neuromuscular junction fragmentation, we found that heterozygous and homozygous knockout animals have a significantly higher probability of being fragmented compared to control animals (see Figures 6 and 7).
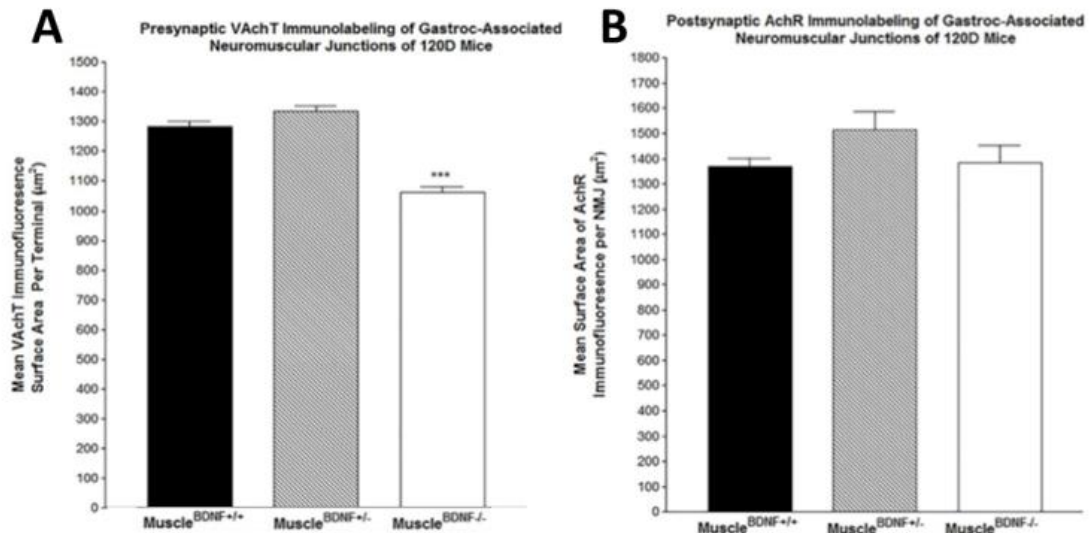
Figure 5. Mean VAChT immunofluorescence at the presynapse and postsynapose of gastroc-associated neuromuscular junctions of 120d mice. There is a significant decrease in presynaptic VAChT immunofluorescence in homozygous knockouts compared to controls (A). There are no significant changes in postsynaptic VAChT immunofluorescence across genotypes (B).
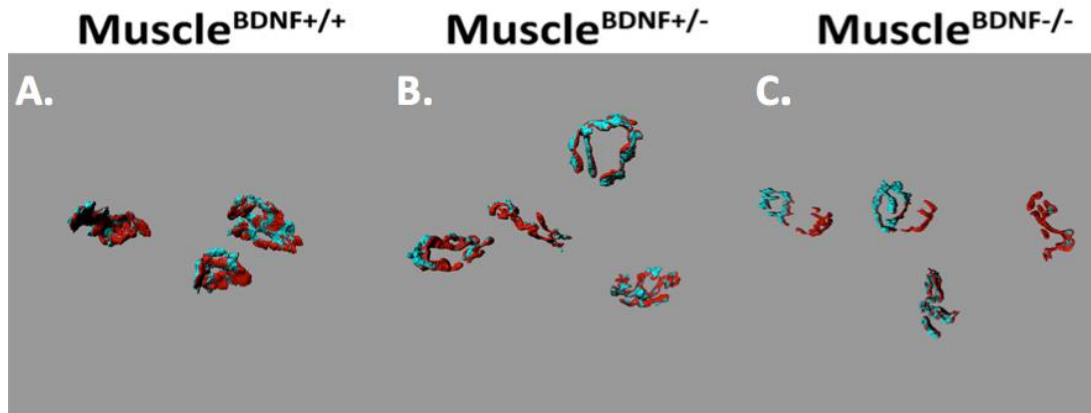
Figure 6. Representative photomicrograph of neuromuscular junction fragmentation in animals lacking skeletal muscle-synthesized BDNF. Control animals show complete, whole neuromuscular junctions (A) with presynaptic VAChT in cyan and postsynaptic AChR in red. Heterozygous and homozygous knockouts show genotype dependent increases in neuromuscular junction fragmentation (B and C respectively).
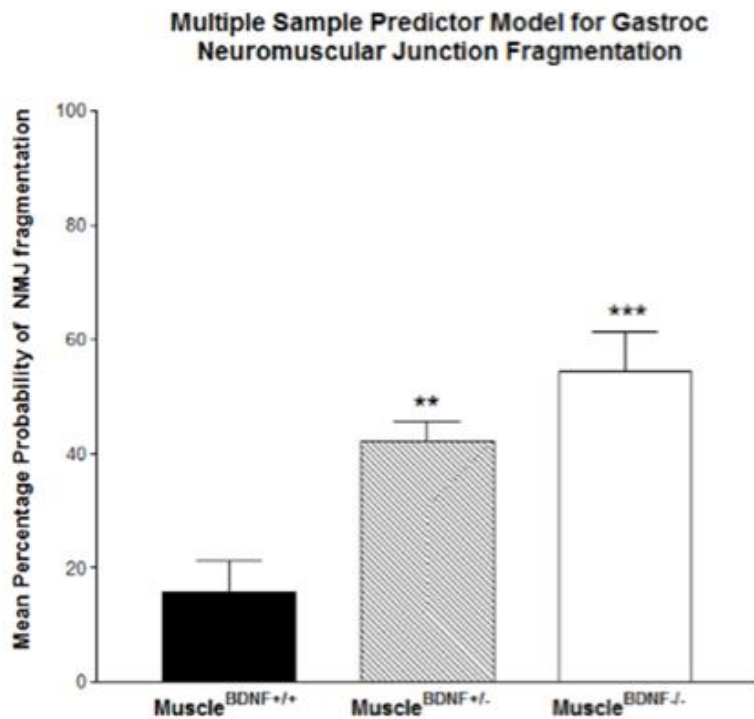
Figure 7. Mean probability of gastroc neuromuscular junction fragmentation according to multiple sample predictor model. Heterozygous and homozygous knockout animal gastroc-associated neuromuscular junctions have a significantly higher probability of being fragmented compared to controls.

We have also observed gastroc-associated motorneuron pathology, including decreased soma size, decreased dendritic diameter, and what appeared to be a decrease in dendritic length in 120d mice lacking muscle-synthesized BDNF (Pomeroy, 2013).
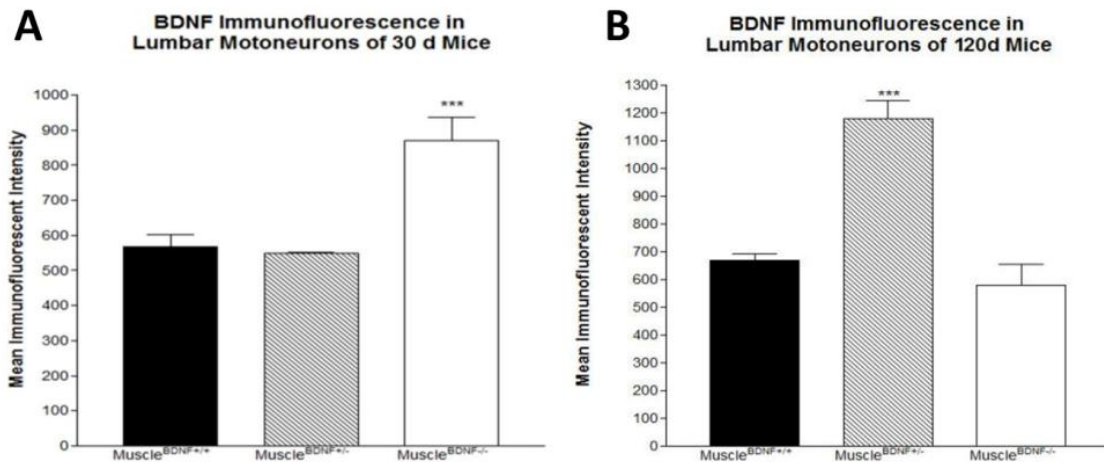
Figure 8. Mean BDNF immunofluorescence in lumbar motorneurons of 30d and 120d mice. 30d homozygous knockout animals show significantly higher BDNF immunofluorescence in the soma of lumbar motorneurons compared to control animals (A), while heterozygous knockouts show no change. At 120d, BDNF immunofluorescence in significantly increased in the lumbar motorneuron somas of heterozygous knockouts, while homozygous knockouts show no change compared to control animals (B).

A Mean Lamina X Motoneuron Cell Soma Area in 30d Animals

B Mean Lamina X Motoneuron Cell Soma Area in 120d Animals
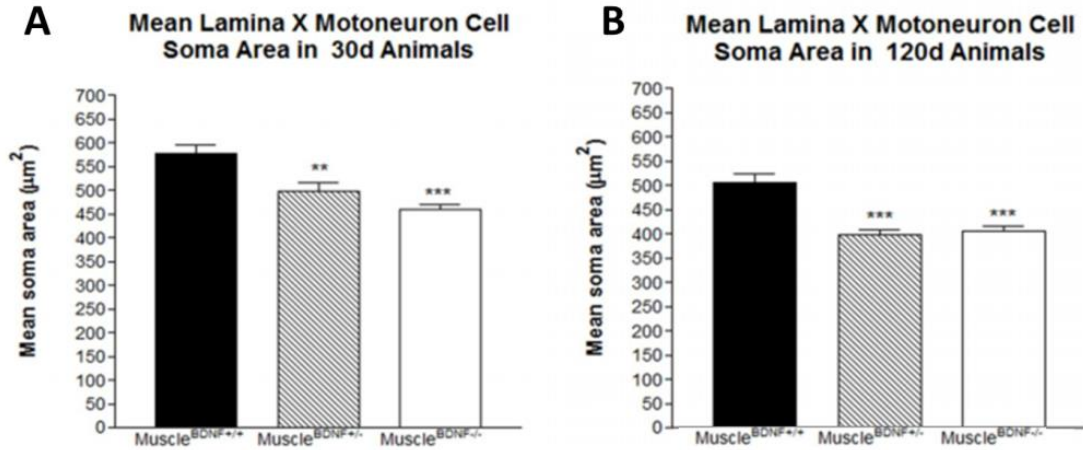
Figure 9. Mean lamina X motorneuron cell soma area in 30d and 120d animals. Heterozygous and homozygous knockout animals show a significant decrease in mean motorneuron soma area compared to controls at both 30d and 120d (A and B respectively).
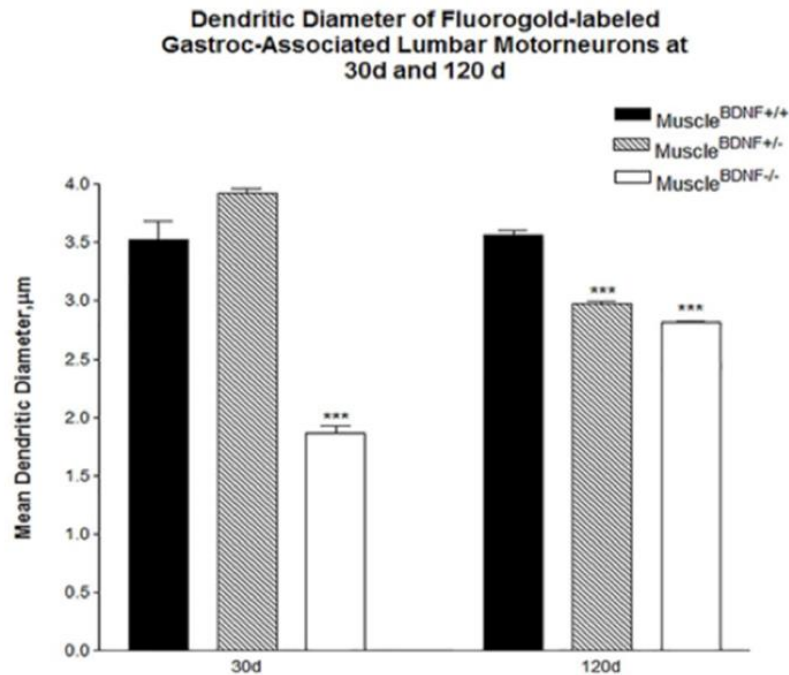
Figure 10. Mean dendritic diameter of fluorogold-labeled gastroc-associated lumbar motorneurons at 30d and 120d. Homozygous knockouts show significantly decreased mean dendritic diameter compared to controls at both 30d and 120d. Heterozygous knockouts show significantly decreased mean dendritic diameter compared to control animals at 120d only.

Dendritic Length of Fluorogold-labeled Gastroc-Associated Lumbar Motorneurons at 30d and 120 d
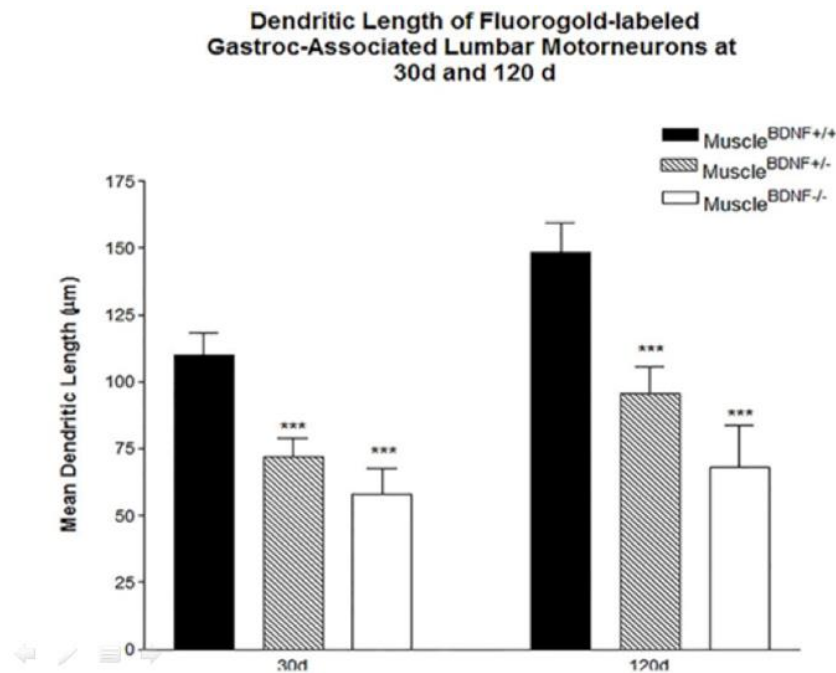
Figure 11. Mean dendritic length of fluorogold-labeled gastroc-associated lumbar motorneurons at 30d and 120d. Homozygous and heterozygous knockout animals show decreased mean dendritic length compared to controls at both 30d and 120d.

Because the mean dendritic length in Muscle[BDNF+/-] and Muscle[BDNF-/-] gastroc-associated motorneurons was shorter than typical dendritic length in Muscle[BDNF+/+] controls, we chose to investigate potential deficits in retrograde transport in gastroc-associated motorneuron axons. We reasoned that we may have uncovered deficits in retrograde transport mechanisms, and not an actual reduction in dendritic length based on the method by which we measured dendritic arborization. We utilized the commercially available retrograde tracing molecule Fluorogold[TM] (Fluorochrome Inc., Denver, CO) to label gastroc-associated neurons. Following injection of Fluorogold into the gastroc, the

13

tracer molecule is endocytosed by innervating motorneurons and transported in vesicles retrogradely along the axon microtubules to the neural soma where it diffuses into the cytoplasm and into the dendritic arbors (Catapano et al., 2008). Disruption of retrograde transport mechanisms could explain the decrease in Fluorogold labeling in the motorneuron dendrites in our Muscle$^{BDNF+/-}$ and Muscle$^{BDNF-/-}$ animals (Pomeroy, 2013).

Retrograde transport relies on the molecular motor dynein. The heavy chains found in dynein include motor domains that interact with microtubules and generate the force necessary to move forward via ATP hydrolysis. Dynein is made up of heavy motor domains protein chains that interact with microtubules and generate the force necessary to move forward via ATP hydrolysis. Other important subunits of dynein include intermediate chains, light intermediate chains and light chains, all of which are required to interact with the cargo being transported. A second protein, dynactin-1 (DCTN1), plays an important role in initiating axonal transport (Cosker and Segal, 2014). The DCTN1 adaptor protein complex contains a central scaffold protein subunit known as actin-related protein 1 (Arp1) that interacts with transport vesicles and other cargos, and a sidearm containing a p150^{glued} subunit that interacts directly with dynein intermediate chains and associates with microtubules (see Figure 12).
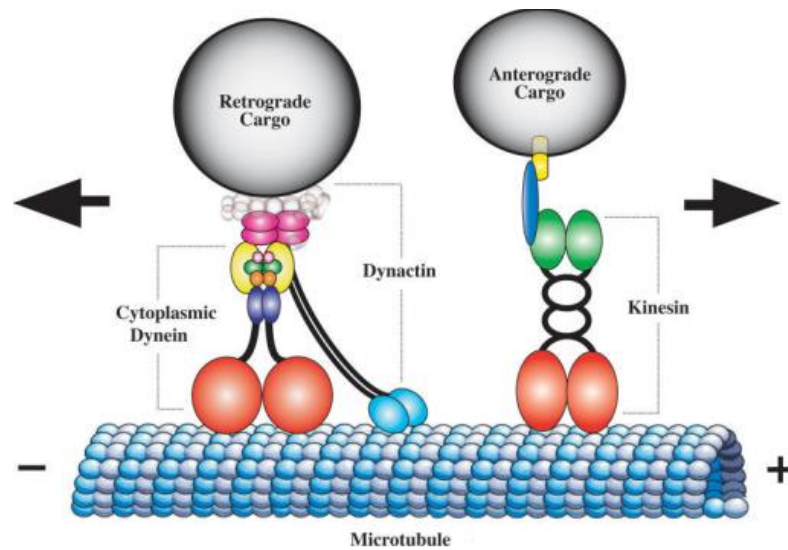
Figure 12. Adapted from Duncan and Goldstein, 2006: Cytoplasmic Dynein and Kinesin Power Axonal Transport. Schematic diagram of the microtubule motor proteins cytoplasmic dynein and kinesin. Cytoplasmic dynein transports cargo in the retrograde direction toward the minus ends of microtubules whereas kinesin transports cargo in the anterograde direction toward the plus ends. Cytoplasmic dynein is a large multimeric protein complex comprising two heavy chain subunits (red) that possess microtubule binding and ATPase activity, two intermediate chains (yellow), two light intermediate chains (indigo), and an assortment of light chains (light pink, green, orange) (reviewed in [7]). Dynactin, a large multisubunit protein complex of comparable size to cytoplasmic dynein, is proposed to link the dynein motor to cargo and/or increases its processivity. The largest dynactin subunit, p150^{Glued} (turquoise), forms an elongated dimer that interacts with the dynein intermediate chain and binds to microtubules via a highly conserved CAP-Gly motif at the tip of globular heads. The dynactin subunit p50 (dark pink) occupies a central position linking p150^{Glued} to cargo. The conventional kinesin holoenzyme, also known as kinesin-1, is a heterotetramer comprising two Khc subunits (red) with microtubule binding and ATPase domains, a central coiled stalk, and a tail domain that interacts with two Klc subunits (green). Klcs may mediate cargo binding via an intermediate scaffold protein (blue) that binds a cargo transmembrane protein (yellow).

Yano et al., show that TrkA, B, and C neurotrophin receptors are found in a complex with the dynein light and intermediate light chains, supporting dynein-based transport of TrkB-containing signaling vesicles to the neural soma from the presynaptic terminal (Yano et al., 2001). The signaling endosome hypothesis, reviewed by Cosker

and Segal (2014), is a leading hypothesis describing the mechanisms involved in transport of Trk-BDNF complexes form the axon terminal to the cell soma (see Figure 13 for a depiction of the signaling endosome model). In this model, once BDNF binds to a Trk receptor, the receptor subsequently autophosphorylates and recruits signaling molecules including PLCγ, PI3K and Ras. PI3K-Akt activity has been implicated in regulating GTPases, dynamin, Rab5, and adapter protein 2 (AP2), all of which are involved in the process of endocytosis. Furthermore, inhibition of PI3K-Akt activity leads to decreased accumulation of NGF-TrkA signaling endosomes in the cell body. Increased Ca^{2+} mobilization via IP3 signaling, a downstream effector of PLCγ, activates calcineurin, a phosphatase that dephosphorylates dynamin in neurons. Dephosphorylation of dynamin is critical for NGF-TrkA endocytosis (Cosker and Segal, 2014). Erk1 activation via the Ras-MAP kinase pathway has been shown to initiate recruitment of dynein to the signaling endosome by phosphorylating dynein intermediate chains (IC), specifically the neuronally expressed IC-1B isoform which selectively binds to and transports TrkB-BDNF signaling endosomes (Cosker and Segal, 2014). Ligation experiments showing that activated Trk receptors accumulate distal to the ligation site supports the idea that Trk receptors are retrogradely transported. Furthermore, studies have shown that phosphorylated Trk receptor localization to the cell body is critical for nuclear responses to neurotrophic activation (Ginty and Segal, 2002).
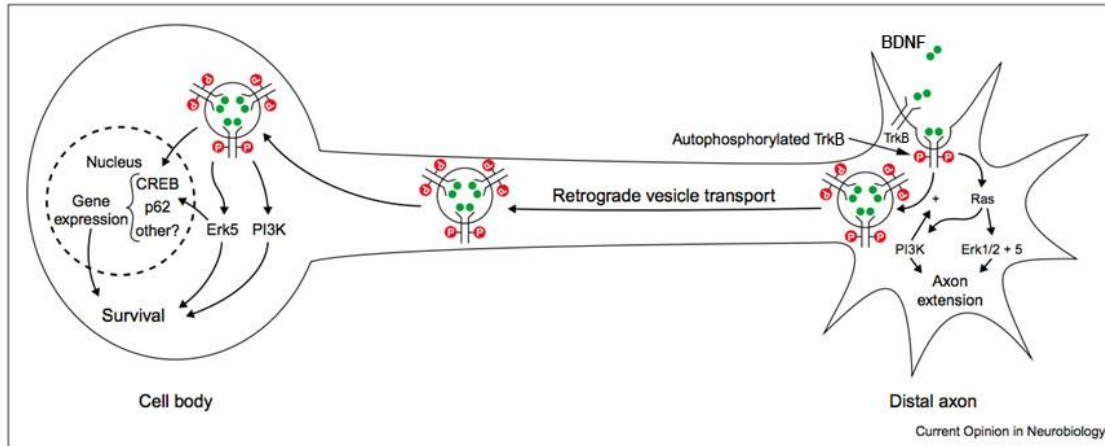
Figure 13. Adapted from Ginty and Segal, 2002: The 'signaling endosome' model. Trk receptors on distal axons are activated upon binding to neurotrophin. The ligand–receptor complex internalizes through clathrin-mediated endocytosis. Some of the vesicles become specialized endosomes that serve as platforms for continued Trk signaling and are transported retrogradely to the cell body using a dynein-dependent and microtubule-dependent transport mechanism. The vesicle-associated Trk receptor remains autophosphorylated and capable of promoting a unique set of signals upon arrival at the cell bodies. These include PI3K and Erk5.

Disruption of retrograde transport mechanisms is indeed a characteristic of multiple neurodegenerative diseases. Huntington's disease (HD) is caused by a polyglutamine tract expansion in the huntingtin (HTT) gene and is characterized by the degeneration of striatal neurons (Gharami et al., 2008). Striatal neurons do not synthesize BDNF themselves, and rely on postsynaptic cortical neurons for neurotrophic support (Altar et al., 1997). BDNF levels are decreased in striatal neurons and several therapeutic approaches are based on restoring this vital neurotrophic support (Borrell-Pages et al., 2006; Dompierre et al., 2007; Gharami et al., 2008; Liot et al., 2013; Pineda et al., 2009; Roux et al., 2012; Zala et al., 2008). Gharami et al., show that overexpression of BDNF in the forebrain of mice expressing mutant HTT restores BDNF-TrkB signaling activity and ameliorates motor dysfunction and other HD phenotypes (2008). In untreated mutant

HTT animals, anterograde and retrograde transport of BDNF is disrupted in corticostriatal neurons. In this model, not only are striatal neurons receiving reduced amounts of BDNF, but the retrograde transport of activated TrkB receptors at striatal dendrites is defective (Liot et al., 2013; Zala et al., 2008). It is now known that HTT plays a critical role in the transport of retrograde vesicles, including those containing BDNF, by binding to TrkB, which also is in a complex with dynein. Silencing HTT in cultured striatal neurons results in a decrease of TrkB transport and subsequent TrkB induced signaling (Liot et al., 2013). Treatment that restores BDNF transport in corticostriatal neurons in HD animal models effectively reduces associated pathology in the effected striatal neurons (Dompierre et al., 2007; Pineda et al., 2009; Roux et al., 2012; Zala et al., 2008).

In another example, SBMA, a neurodegenerative disease caused by a polyglutamine tract expansion in the androgen receptor (AR) gene, is also characterized by deficits in retrograde transport in affected neurons, in this case bulbar and spinal motorneurons. Katsuno et al. illustrate that transcriptional dysregulation of DCTN1, a critical component of the retrograde transport complex, plays a critical role in defective axonal transport and results in the motorneuron pathology associated with SBMA progression (Katsuno et al., 2006). This group further shows that affected motorneurons have decreased levels of DCTN1 mRNA. Importantly, when DCTN1 is overexpressed in motorneurons of the same animals, neuronal dysfunction is reversed. With polyglutamine tract disorders like HD and SBMA, it is thought that neuronal dysfunction is, in large part, caused by pathogenic proteins accumulating in the cell leading to the sequestration of heat shock proteins, proteosomal components, transcriptional factors and

coactivators (Katsuno et al., 2006). Katsuno et al., showed that castration of affected mice, which would prevent mutant AR from accumulating, reversed the disruptions in DCTN1-regulated retrograde transport.

Disruptions in retrograde transport are not limited to models of polyglutamine tract disorders such as HD and SBMA. ALS is a neuromuscular disease characterized, in part, by axonal transport deficits (Ikenaka et al., 2013; LaMonte et al., 2002). 90% of ALS cases are sporadic (sALS), while only ten percent of documented cases are caused by dysfunction or dysregulation of a specific gene and are subsequently referred to as familial ALS (fALS). Therefore, defective axonal transport in the vast constellation of points of cellular dysregulation associated with sALS must be attributed to a mechanism other than the accumulation of proteins that is a hallmark of polyglutamine tract expansion diseases. There is evidence that patients with sALS have a significant decrease in DCTN1 mRNA in motorneurons (Münch et al., 2005). There have also been animal studies utilizing DCTN1-knockout/disruption models indicating that a reduction in DCTN1 in motorneurons results in transport deficits and an ALS-like phenotype (Ikenaka et al., 2013; LaMonte et al., 2002). While motorneuron dysfunction in sALS may not be due to accumulation of a specific pathogenic protein, it may be attributed, in part, to accumulation of cellular material that is not retrogradely transported from the motorneuron terminal (Ikenaka et al., 2013). Ikenaka et al., showed that DCTN1 knockdown disrupts transport of autophagosomes and results in dysregulation of normal protein degradation and organelle turnover. While these effects are observed in the motorneurons of patients with and murine models of sALS, the underlying causes are still unknown. Understanding the importance of BDNF-induced signaling in the health and

maintenance of motorneurons, we hypothesized that loss of skeletal muscle-synthesized

BDNF results in altered cell signaling and transcriptional dysregulation that in turn leads

to disrupted axonal transport mechanisms.

In addition to disruptions in neuronal transport mechanisms, various

mitochondrial dysfunctions are common to several neurodegenerative diseases including

HD, SBMA and ALS (Cai and Sheng, 2012; Cassina et al., 2008; Chang and Reynolds,

2006; Martin et al., 2007; Orr et al., 2008; Piccioni et al., 2002; Shi et al., 2010;

Shirendeb et al., 2011). Some of the mitochondrial pathologies observed in sALS and

fALS include disrupted mitochondrial transport in the anterograde, or anterograde and

retrograde directions, mitochondrial fragmentation, and impairments in mitochondrial

fusion and fission events which are important for the constantly changing and carefully

regulated mitochondrial distribution in the cell (Magrané et al., 2009; Vos et al., 2007).

Mitochondrial trafficking is disrupted in HD and SBMA models as well (Chang and

Reynolds, 2006; Orr et al., 2008; Piccioni et al., 2002). Mitochondria have multiple roles

in maintaining a healthy neuron and include ATP synthesis, calcium buffering, and

regulation of apoptosis, among other roles. Mitochondria are not homogenous in their

dispersal throughout the neuron, but instead are denser in areas with higher energy

demands. The presynapse has high energy and calcium buffering demand (de Moura et

al., 2010; Nguyen et al., 1997; Palay, 1956; Su et al., 2010). Mitochondria are required to

fuel events at the neuromuscular junction: vesicle docking, neurotransmitter release,

AChR insertion into postsynaptic membrane, and neurotransmitter re-uptake to name a

few. Mitochondrial trafficking and distribution is carefully regulated in neurons, whose

energy requirements are in constant flux, thus, it is easy to understand how disruptions in axonal transport could lead to mitochondrial pathology.

Interestingly, Su et al., show that BDNF signaling mediates mitochondrial recruitment to the presynapse in hippocampal neurons cultured from Sprague-Dawley rats (Su et al., 2014). They report that increased levels of calcium at the presynapse via the PI3K and PLCγ pathways, activated by BDNF binding to its receptor TrkB, is responsible for the mitochondrial docking. Because BDNF plays a crucial role in the health and maintenance of neurons, and because decreased BDNF levels and mitochondrial deficits are characteristic of several neurodegenerative diseases, we sought to investigate the role of skeletal muscle-synthesized BDNF in motorneuron mitochondrial dynamics, specifically assessing mitochondrial density at the neuromuscular junction.

CHAPTER TWO: GENERATION OF EXPERIMENTAL TRANSGENIC ANIMALS

Introduction

We utilized Cre-Lox gene recombination technology to generate transgenic mice lacking either one or both copies of the BDNF gene in skeletal muscle. We maintained two distinct colonies of transgenic mice. In one transgenic colony, the coding region of the BDNF gene was flanked by 34-basepair LoxP sites. The second colony contained the Cre-recombinase gene transgene driven by a human skeletal actin (HSA) promotor on the X-chromosome. When crossed, the cre-recombinase enzyme, synthesized specifically in skeletal muscle due to the HSA promotor, removed the BDNF coding region located between the two LoxP sites (Miniou et al., 1999). Because the $Cre^{+/+}$ genotype is lethal, we maintained $Cre^{-/-}$ and $Cre^{+/-}$ animals only. For each experiment performed, we used wildtype control ($Muscle^{BDNF+/+}$) animals, heterozygous knockout ($Muscle^{BDNF+/-}$) animals, and homozygous knockout ($Muscle^{BDNF-/-}$) animals. The mating scheme used to generate these animals is detailed in the next section. Figure 14 provides a depiction the Cre-Lox technology used in this model, and Figure 15 provides the results of a long PCR reaction demonstrating that the BDNF gene is indeed knocked out of skeletal muscle in our experimental mice.
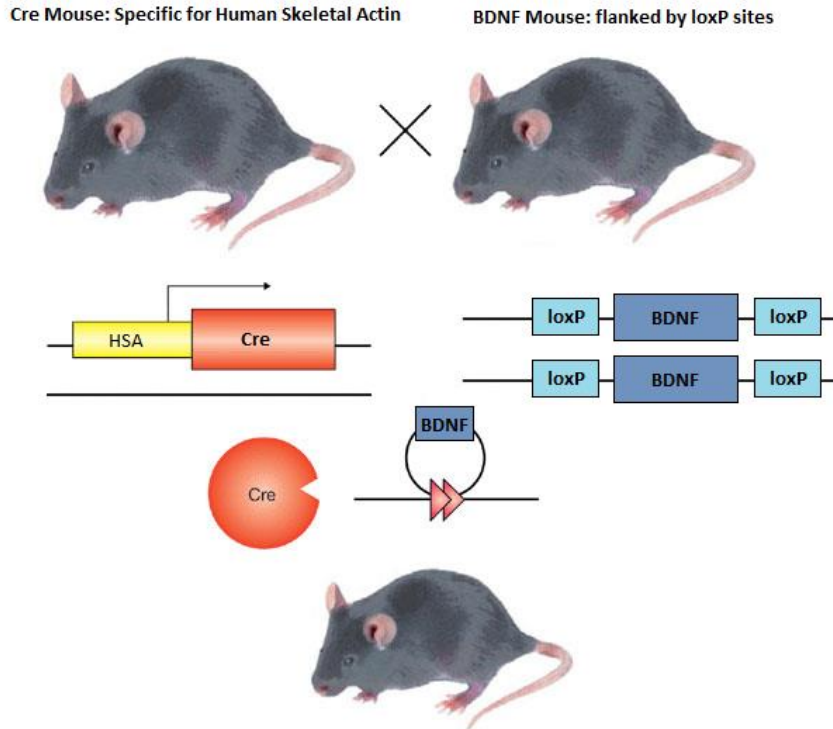
Figure 14. Removal of BDNF gene in skeletal muscle using Cre-Lox gene technology. A mouse transgenic for the Cre recombinase gene driven by the human skeletal actin (HSA) promoter is crossed with a mouse with loxP sites flanking the BDNF gene. Animals that inherit the Cre recombinase gene synthesize the cre recombinase enzyme in skeletal muscle which subsequently excises the sequence between the loxP sites.
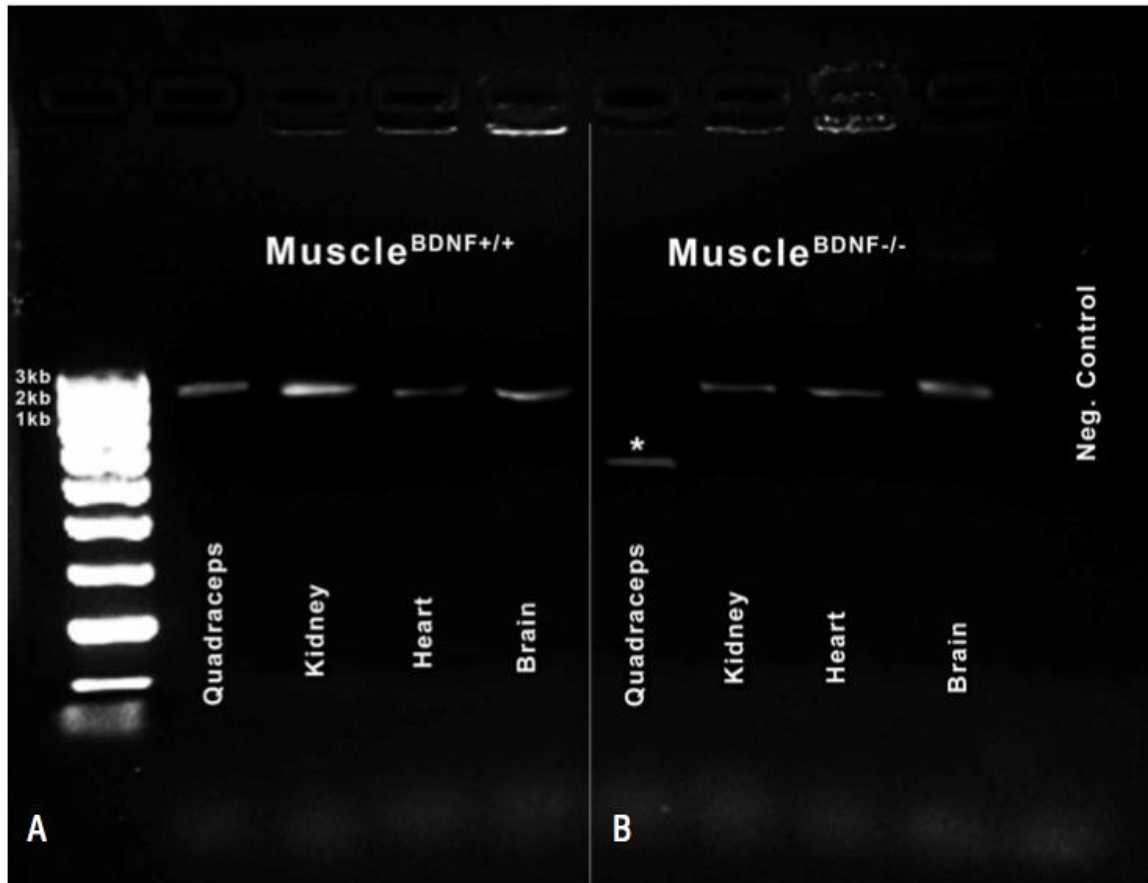
Figure 15. Photograph of amplified BDNF gene PCR assay on agarose gel. Control animals had amplified the full-length coding region of the BDNF gene in skeletal muscle (2050 bp), kidney, heart and brain tissue (A), while the BDNF gene amplification product is shorter in only the skeletal muscles of Muscle[BDNF-/-] mice (975 bp) (B).

Methods

Animals were maintained according to the *NIH Guidelines for the Care and Use of Laboratory Animals* and the Institutional Animal Care and Use Committee of Northern Michigan University. Animals were housed in a temperature- and light-controlled room (14-h light:10hr dark cycle; lights on at 0700 h). Animals had access to Mazuri Rodent Chow (Land O' Lakes Purina Feed LLC, Richmond, IN) and water ad libitum.

Generation of heterozygous knockouts

Males containing LoxP-flanked (floxed) BDNF (BDNF$^{lox+/+}$, Cre$^{-/-}$) were crossed with females containing the Cre-recombinase gene (BDNF$^{lox-/-}$, Cre$^{+/-}$). Parental genotpes were determined using PCR techniques depicted in Figure 17. The resulting F1 offspring were heterozygous for floxed BDNF (BDNF$^{lox+/-}$) and either heterozygous for Cre (BDNFlox$^{+/-}$, Cre$^{+/-}$) or did not contain the cre gene (BDNF$^{lox+/-}$, Cre$^{-/-}$). Males with BDNF$^{lox+/-}$, Cre$^{+/-}$ genotype were used as our heterozygous knockouts. Females with BDNF$^{lox+/-}$, Cre$^{+/-}$ genotype were used as breeders for our F2 animals.

Generation of homozygous knockouts and controls

BDNF$^{lox+/-}$, Cre$^{+/-}$ females were crossed with BDNF$^{lox+/+}$, Cre$^{-/-}$ males. From the resulting F2 offspring, we used BDNF$^{lox+/+}$, Cre$^{+/-}$ animals as our homozygous knockouts, and BDNF$^{lox+/+}$, Cre$^{-/-}$ animals were used as our controls. Figure 16 depicts this mating scheme.
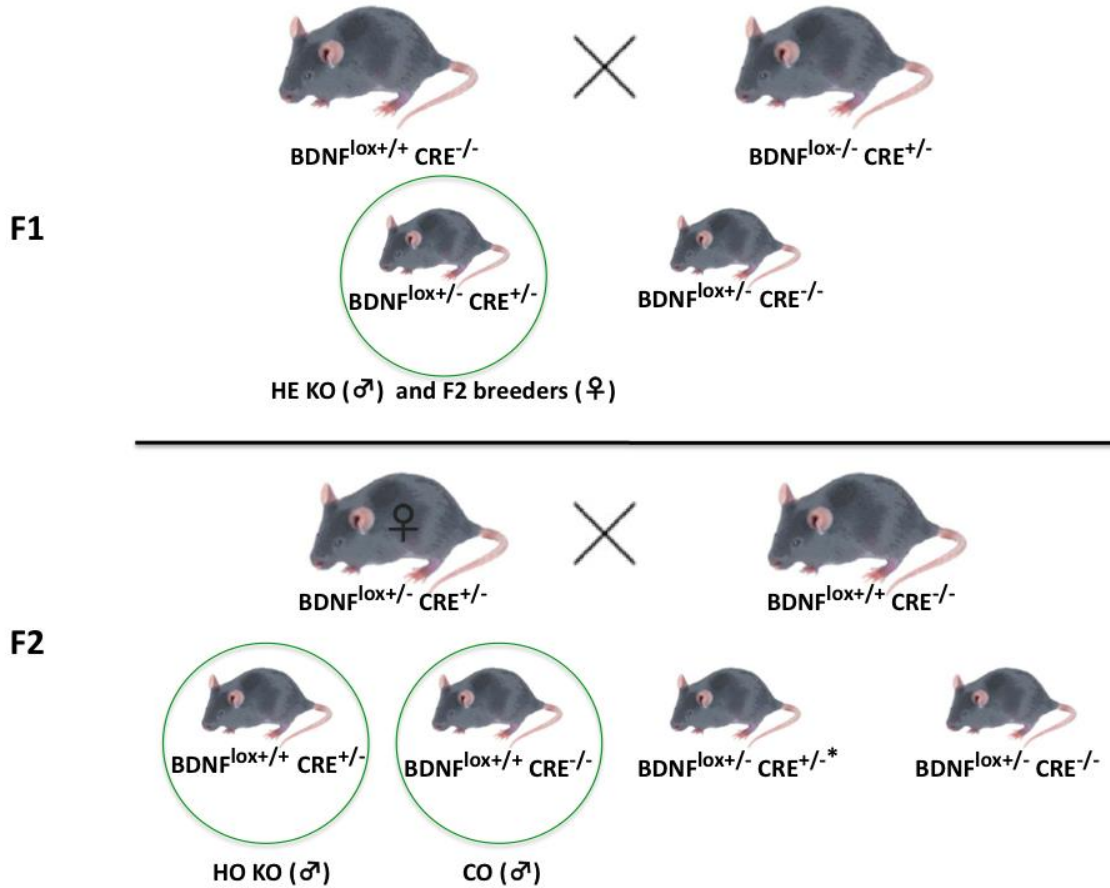
Figure 16. Generation of skeletal muscle-synthesized BDNF knockout animals and controls. In an F1 cross, an animal with a floxed BDNF gene was crossed with an animal that contained a copy of the Cre recombinase gene. As a result, all F1 offspring had one copy of floxed BDNF, while only a proportion contained a copy of the Cre recombinase gene. Males with the $BDNF^{lox+/-} CRE^{+/-}$ genotype were used as experimental heterozygous knockout (HE KO) animals, and females of the same genotype were used as F2 breeders. In the F2 cross, female $BDNF^{lox+/-} CRE^{+/-}$ animals were crossed with males with the floxed BDNF gene. Our homozygous knockout (HO KO) animals and controls were generated from this F2 cross. *The F2 cross also generated HE KO animals, however the F1 crosses yielded sufficient HE KO animals for our experiments.

Genotyping Procedure

After weaning at 21d, a tissue sample was collected from each animal's ear and used for genotyping via PCR and gel electrophoresis. To determine the presence or

absence of floxed BDNF alleles, two specific primers were used, one that binds upstream

of the first loxP site, and a second that binds in the middle of the gene coding region.

Floxed and non-floxed BDNF are distinguishable based on the size difference of their

amplification products: the non-floxed and floxed BDNF products are 437bp and 487bp

respectively. In a separate reaction, a second set of primers were used to determine the

presence of the 100bp CRE gene. Because the CRE gene is not normally found in mice,

we used a pair of primers for a 300bp housekeeping gene along with a pair of primers

that recognized CRE which served as a positive control. When amplification product was

run through a gel, one band represented the housekeeping gene found in all of the

animals, and a second, shorter, band represented the CRE gene if it was present. See

Figure 17 for an example of both CRE and BDNF PCR amplification products run

through agarose gel.
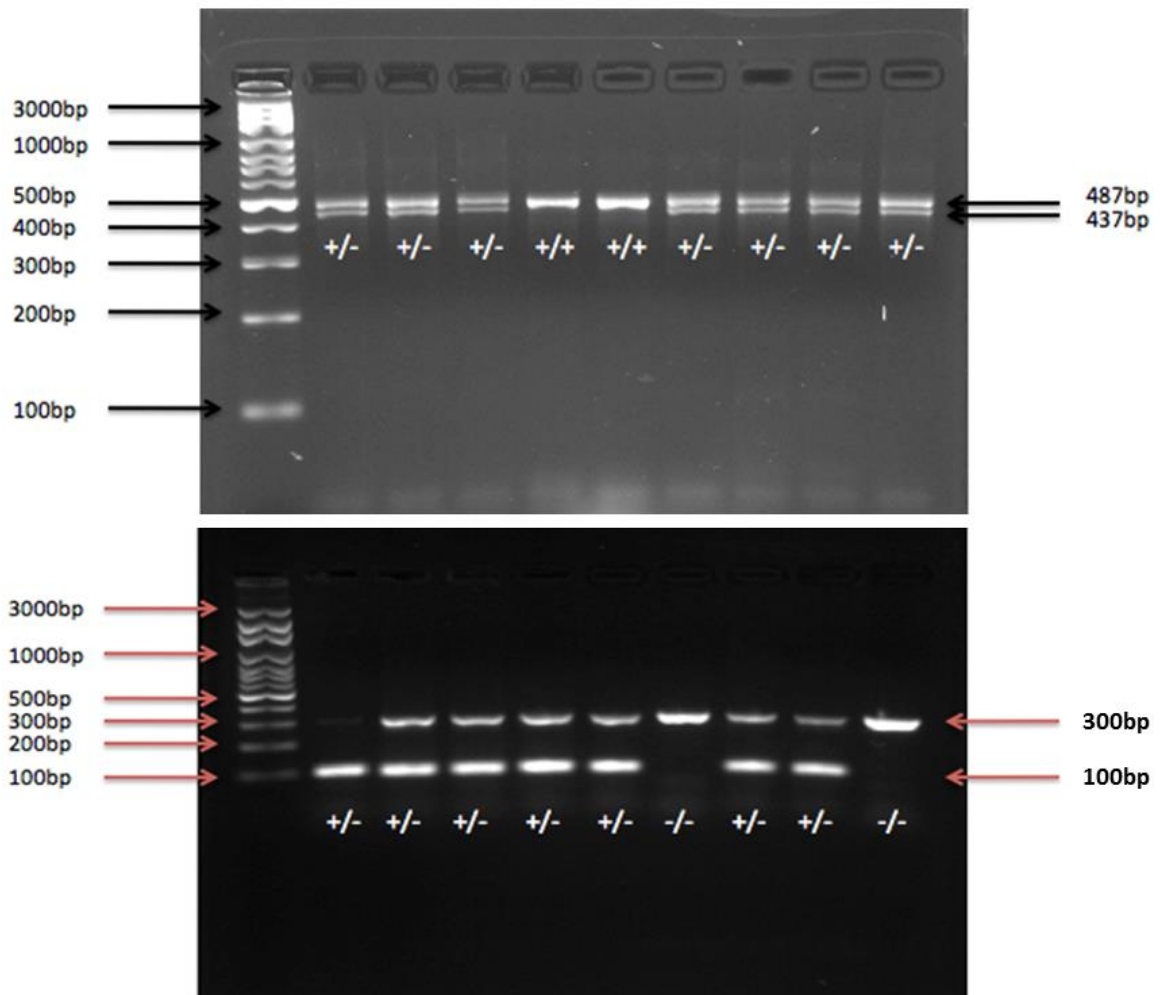
Figure 17. Representative photographs of the BDNF and CRE gene PCR on an agarose gel. The bottom band in bottom panel represents the CRE gene (100bp), while the top band is a housekeeping gene that all animals should have (300bp). The bottom band in the top panel represents BDNF that is not floxed (437bp), while the top band represents BDNF that is floxed (487bp). This information combined allowed us to determine the genotypes of our animals.

CHAPTER THREE: ASSESSMENT OF PHOSPHORYLATED NEUROFILAMENT-H PROTEIN ACCUMULATION AT THE DISTAL AXON IN GASTROCNEMIUS-ASSOCIATED MOTORNEURONS IN MUSCLE SYNTHESIZED-BDNF KNOCKOUT ANIMALS

Introduction

Neurofilaments in the mature nervous system provide neuronal structure, and play an important role in increasing axonal caliber and thus increasing conduction velocity in myelinated axons (Lazer-Azogui et al., 2015). Neurofilament subunits NF-L, NF-M and NF-H all contain an α-helical rod domain, an N-terminal head domain, and a C-terminal tail domain. The main difference between these three subunits is the length of the C-terminal tails, with NF-L having the shortest and NF-H the longest tail domains. The rod domains of the subunits interact with each other to form dimers, protofilaments, and filaments. NF-L dimerizes with either NF-M or NF-H, and homodimers are not common (Lazer-Azogui et al., 2015). The phosphorylation state of serine residues on the NF-L subunit head domains regulates polymer assembly, with phosphorylation of the head domains inhibiting assembly of NF-L (Yates et al., 2009). Phosphorylation of the C-terminal tails regulates axonal transport of the neurofilaments (Shea et al., 2009). Neurofilament subunits synthesized in the cell body are transported into the axon as subunit assemblies, short filaments or both. Neurofilament subunit assemblies are predominately observed in the proximal axon while short filaments are predominately observed in the distal axon, suggesting that filament assembly occurs during axonal transport (Lazer-Azogui et al., 2015). C-terminal-phosphorylated neurofilament subunits are localized in axons, while the cell body and dendrites contain non-phosphorylated neurofilaments (Sternberger and Sternberger, 2003). Phosphorylation of the N-terminal

29

head domain on NF-M has been shown to inhibit phosphorylation of the C-terminal tail domain, suggesting that dephosphorylation of the head domain in the cell body precludes phosphorylation of the tail domain and subsequent transport of the tail domain-phosphorylated subunits into the axon (Zheng et al., 2003).

It has been suggested that there are three pools of neurofilaments in the axon: a pool of neurofilaments associated with molecular motors (kinesin or dynein), a pool of neurofilaments not associated with motors, and a pool of neurofilaments linked with other neurofilaments (Shea et al., 2009). Motil et al., (2007) show that neurofilaments are increasingly phosphorylated as they are transported anterogradely along the axon. They show that the increased phosphorylation state of the neurofilament subunit decreases its affinity for the anterograde motor kinesin, and increases its affinity for the retrograde motor dynein. Supporting this, while studying overall anterograde transport rates of NF-H subunits in axons, Lewis and Nixon (1988) showed that the least phosphorylated NF-H subunits travel twice as fast as hyperphosphorylated NF-H subunits. Additionally, Ackerly et al., (2013) observed that extensively phosphorylated neurofilaments pause more often than non-phosphorylated neurofilaments. It has also been observed that C-terminal phosphorylation promotes neurofilament-neurofilament associations, indeed phosphatase inhibition increases neurofilament bundle size. Furthermore, phosphorylation of the C-terminal has been shown to cause this tail domain to extend laterally from the neurofilament subunit, linking it to other neurofilament subunits (Shea et al., 2009). It is important to note that the long C-terminal tails of NF-M and NF-H subunits have several phosphorylation sites at lysine-serine-proline (KSP) residues. In humans for example, the NF-M subunit has 13 KSP sites in the tail domain,

and NF-H has 43-44 depending on the allele (Rudrabhatla et al., 2010). Therefore, phosphorylation of the C-terminal domains of NF-H, and to a lesser extent NF-M, is going to play the largest role in regulation of neurofilament-motor and neurofilament-neurofilament associations.

There are two contrasting models regarding axonal transport of neurofilaments (Lazer-Azogui et al., 2015). One model, the "stop and go" model, depicts the neurofilament makeup of the axon as being highly dynamic, with neurofilaments constantly rotating between the three pools described above. Conversely, the second, "stationary," model suggests that 10% of axonal neurofilaments are in movement, while the remaining 90% is fixed and may remain so for months. Both models account for a subset of neurofilament subunits in motion, by kinesin and dynein motors. The retrograde transport of neurofilament subunits by dynein/dynactin has been shown to be important for the health of the neuron. Indeed, depletion of dynein *in vitro* leads to accumulation of neurofilaments at the neurite tip (He et al., 2005). Furthermore, targeted disruption of dynein/dynactin function *in vivo* leads to neurofilament aggregates at distal axons (LaMonte et al., 2002). We hypothesized that dynactin expression is dysregulated in motorneurons due to decreased skeletal muscle-synthesized BDNF/TrkB signaling events in motorneurons. Furthermore we expected to see an accumulation of NF-H at the distal axon of gastroc-associated motorneurons in our heterozygous and homozygous knockout animals.

We used an antibody that binds specifically to a phosphorylated epitope in extensively phosphorylated NF-H (anti-NF-H-P) and to a lesser extent with NF-M. Phosphatase treatment of tissue prevents binding of this antibody (Goldstein et al., 1987;

31

Sternberger and Sternberger, 1983). Utilizing immunohistochemistry techniques, we labeled NF-H-P, synaptophysin (pre-synaptic marker), and α-bungarotoxin (post-synaptic marker) in gastroc-associated neuromuscular junctions. After imaging the immunolabeled neuromuscular junctions, we measured the mean surface area of NF-H-P immunolabeling at the distal axons of gastroc-associated motorneurons of control, heterozygous knockout and homozygous knockout mice.

Methods

Tissue Harvest and Processing

Animals (30d or 120d) were anesthetized using Isofluorane (Henry Schein Animal Health, Melville, New York) and the right gastroc muscle was removed. The muscle was immediately placed in a plastic mold, covered in Tissue-Tek OCT compound (Sakura, Tokyo, Japan) and snap-frozen on dry ice. The animals were then euthanized via I.P. injection of overdose of sodium pentobarbital solution Beuthanasia®-D (Schering Plough Animal Health, city, New Jersey). Frozen muscles were sectioned longitudinally at 40mm, using a Leica CM1850 Cryostat, and mounted onto gelatin-coated slides.

Immunohistochemistry

30d and 120d muscle sections were chemically cross-linked to gelatin-coated slides by incubating in paraformaldehyde (4% in 1:9 0.2M monobasic:0.2M dibasic sodium phosphate buffer, pH 7.4) for 15 min and then rinsed with 1XPBS (14mM sodium chloride, 2.7mM potassium chloride, 1.5mM monobasic potassium phosphate, 8.0mM dibasic sodium phosphate heptahydrate, pH 7.4). After incubating 1hr with

blocking buffer (10% normal donkey serum, 0.2% Triton X-100, 0.01% sodium azide in 1XPBS), 30d and 120d tissue was incubated overnight with anti-NF-P-H 1:1000 (Covance, Princeton, New Jersey), and anti-synaptophysin 1:500 (Abcam, Cambridge, United Kingdom), in blocking buffer. The 30d and 120d tissue was rinsed again with 1XPBS, and incubated for 1 hr with the secondary antibodies Alexa Fluor 594-conjugated α-bungarotoxin 1:1000 (Life Technologies, Carlsbad, California), Alexa-488-conjugated donkey anti-mouse 1:200 (Jackson Laboratories, Bar Harbor, Maine), and Alexa-647-conjugated donkey anti-rabbit 1:200 (Jackson Laboratories) in 1XPBS and 0.2% Triton X-100. The 30d and 120d tissue was rinsed with 1XPBS, air-dried for 4-6hrs, and coverslipped using Vectashield® Mounting Medium with DAPI (Vector Laboratories, Burlingame, California) to prevent quenching.

Imaging and Data Collection

Images were collected using an Olympus Fluoview FV1000 laser scanning confocal microscope. Scanning speed, aspect ratio and step size were set at 20μs/pixel, 800 X 800, and 0.54μm respectively. Image X, Y, and Z coordinate limits were set to include the entire neuromuscular junction in the final Z-stack. 45 junctions per animal per experimental group were imaged for 30d and 120d tissue. Each image was uploaded into IMARIS 3D rendering computer software (Bitplane, Concord, MA). Using the surface tool, 3D surfaces were created for the α-bungarotoxin, synaptophysin and NF-H-P immunofluorescent channels (post-synapse, pre-synapse and axon respectively). Next, each NF-H-P surface was traced, using the measuring tool, for 30μm beginning at the pre-synapse surface. NF-H-P immunofluorescence inside the pre-synapse was unified

with the 30µm segment if present. Finally, surface area measurements were obtained for each 30µm segment. Once all terminal NF-H-P immunofluorescent segments were analyzed (about 45 segments per animal), one-way analysis of variance (ANOVA) and Bonferroni post-test statistics were performed, using GraphPad Prism software, to compare group averages at each age group.

Results

To assess potential deficits in retrograde transport in motorneuron axons of muscle-synthesized BDNF deficient mice, we measured accumulation of NF-H-P at the distal axon of motor neurons innervating the gastroc muscle. Total surface area of NF-H-P immunolabeling in the distal-most 30µm of innervating axons was measured. Preliminary data for 30d animals shows no significant changes in NF-H-P immunolabeling surface area across genotypes (Figure 19A). At 120d there is a significant increase in NF-H-P immunolabeling surface area in the distal 30µm of the axon in both Muscle$^{BDNF-/-}$ and Muscle$^{BDNF+/-}$ animals (p<0.01; Figure 19B). Representative photomicrographs of a control animal and a homozygous knockout animal are provided in Figure 18.
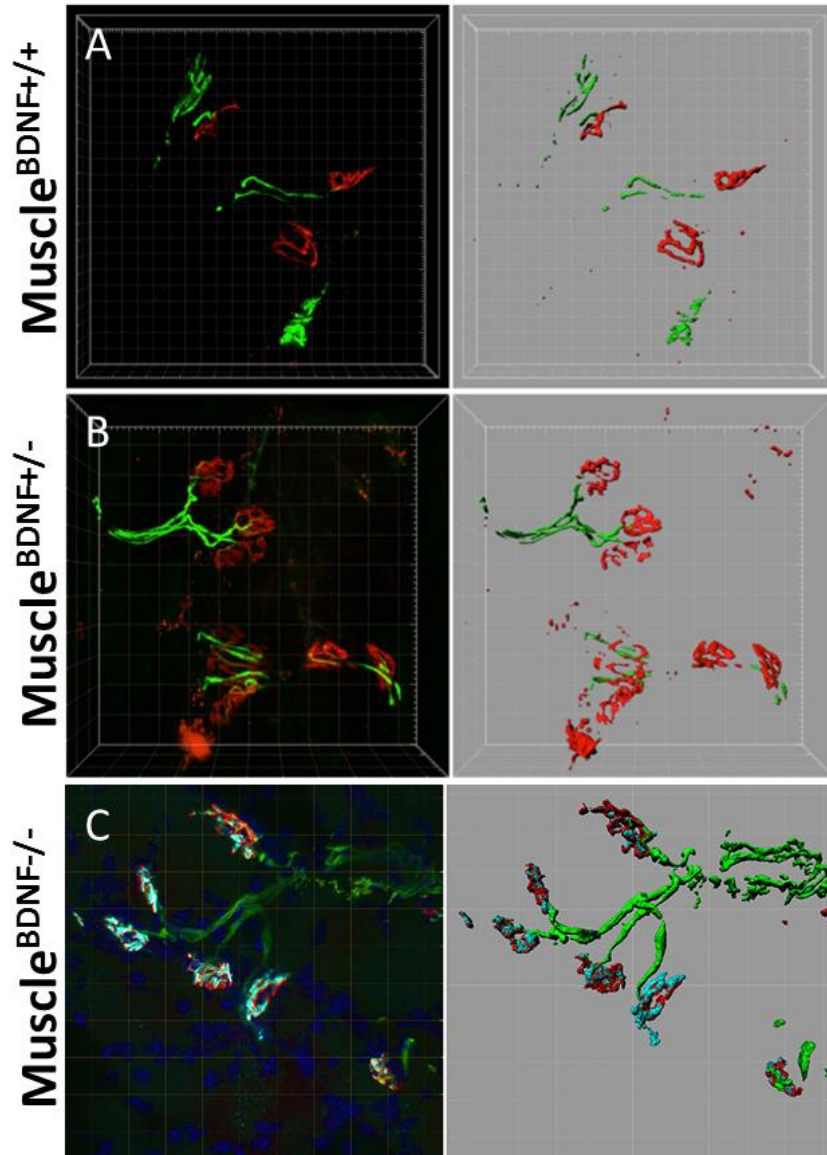
Figure 18. Representative photomicrographs of NF-H-P accumulation in distal axon in animals lacking skeletal muscle-synthesized BDNF. Images include the presynapse labeled with anti-synaptophysin (cyan), postsynapse labeled via α-bungarotoxin (red) and NF-H-P (green). Confocal images on the left are matched with corresponding images rendered using IMARIS software (right). Note the accumulation of NF-H-P in the heterozygous and homozygous knockouts (B and C respectively) compared to controls (A).

A — Immunolabeling of NF-H-P in the Axons of Gastroc-Associated Neuromuscular Junctions in 30D mice

B — Immunolabeleing of NF-H-P in the Axons of Gastroc-Associated Neuromuscular Juctions in 120D Mice
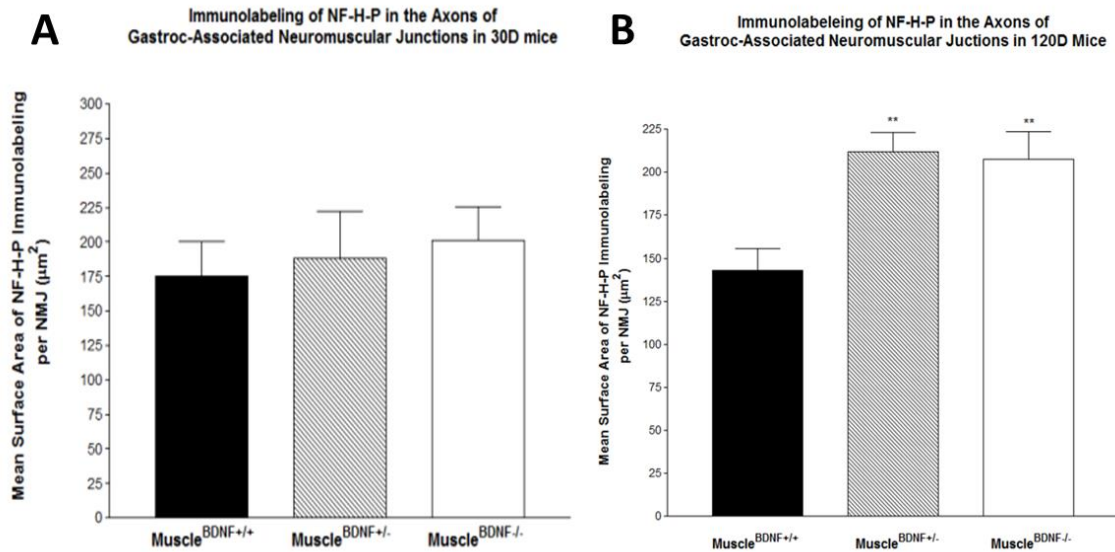
Figure 19. Mean surface area of NF-H-P immunolabeling in distal gastroc-associated motorneuron axons in 30d and 120d mice. At 30d, preliminary data shows no significant changes in mean surface area of NF-H-P immunolabeling in distal axons (n=5 animals per genotype) (A). At 120d, both Muscle$^{BDNF+/-}$ and Muscle$^{BDNF-/-}$ experimental groups show a significantly increased mean surface area in the distal axon when compared to controls (B) (**$p<0.01$; n=7 animals per genotype).

Discussion

To assess potential retrograde transport deficits in 30d and 120d Muscle$^{BDNF-/-}$ and

Muscle$^{BDNF+/-}$ animals, we quantified NF-H-P at the distal axon. Recall that as NF-H is

transported anterogradely through the axon it becomes increasingly phosphorylated.

Hyperphosphorylated NF-H loses affinity for kinesin, and gains affinity for dynein. Thus

by labeling hyperphosphorylated NF-H, we are labeling NF-H that is associated with

dynein, the retrograde motor. An accumulation of NF-H-P at the distal axon would

therefore indicate retrograde transport deficits. At 30d, our preliminary data shows that

there is no significant increase in mean NF-H-P immunofluorescence in the distal 30µm

axon of gastroc-associated motorneurons of homozygous or heterozygous knockout

animals (Figure 19A). This would suggest that NF-H is not accumulating in these animals at this time point. However, we do show significant increases in mean surface area of NF-H-P immunofluorescence in distal gastroc-associated axons in 120d Muscle$^{BDNF-/-}$ and Muscle$^{BDNF+/-}$ mice (Figure 19B) This data indicates a significant accumulation of this retrogradely transported protein in 120d homozygous and heterozygous knockouts, suggesting that there is indeed disruption in retrograde transport along motorneuron axons in 120d mice lacking skeletal muscle-synthesized BDNF. This data is congruous with other motorneuron pathologies we have observed in this animal model. For example, we have previously shown significant decreases in soma area in lamina X motorneurons, dendritic length, and dendritic diameter in Muscle$^{BDNF-/-}$ and Muscle$^{BDNF+/-}$ 120d mice compared to controls (see Figures 9, 10 and 11 respectively; Pomeroy, 2013). These results support our hypothesis that skeletal muscle-synthesized BDNF is important for maintenance of retrograde transport in motorneurons. Indeed, it appears skeletal muscle-synthesized BDNF-TrkB signaling is necessary for the formation of retrograde transport complexes at the distal axon.

CHAPTER FOUR: ASSESSMENT OF RETROGRADE TRANSPORT IN GASTROC-ASSOCIATED MOTORNEURONS VIA SCIATIC NERVE LIGATION EXPERIMENTS

Introduction

Chapter 3 describes how accumulated NF-H-P is present in distal axons of gastroc-associated motorneurons in 120d, but not 30d, Muscle[BDNF-/-] and Muscle[BDNF+/-] animals. Katsuno et al., also found accumulated NF-H-P in motorneuron distal axons when assessing motorneuron retrograde transport in a mouse model of SBMA (Katsuno et al., 2006). The transgenic mice in that study contained an additional 97 CAG repeats in the polyglutamine tract in the AR gene (AR-97Q mice). After finding the accumulated P-NF-H in the motorneuron axons of AR-97Q mice, Katsuno et al., performed a sciatic nerve ligation experiment to further assess hypothesized axonal retrograde transport deficits in the AR-97Q mice (Katsuno et al., 2006). The sciatic nerve is a large bundle of sensory and motorneuron axons that originates in the spinal cord and innervates the lower limbs. Ligating this bundle of axons at mid-thigh while the animal is alive provides a physical barrier to material being transported anterogradely and retrogradely along the axons. Measuring the accumulation of specific materials on each side of the ligation site can help determine potential transport deficits. Katsuno et al., ligated the right sciatic nerve in AR-97Q and control mice for 8 hours. After 8 hours, the animals were euthanized and the sciatic nerve segment that was removed (including 0.5cm on either side of the ligation site) was sectioned (Katsuno et al., 2006). Katsuno et al., then immunolabeled the bi-directionally transported protein synaptophysin, and quantified the synaptophysin-associated immunofluorescence distal or proximal to the ligation site.

38

They found that AR-97Q mice show a significant decrease in synaptophysin immunofluorescence immediately distal to the ligation site compared to that of wild type mice, indicating retrograde transport deficits (Katsuno et al., 2006). To assess potential anterograde transport deficits in these animals, Katsuno et al., measured synaptophysin immunofluorescence directly proximal to the ligation site. They found no significant differences in this segment of the nerve, indicating that the anterograde transport of this protein was not disrupted (Katsuno et al., 2006).

Because both dynein and DCTN1 are necessary for microtubule-dependent axonal retrograde transport, including the retrograde transport of synaptophysin, and because reduction of DCTN1 is a characteristic of several neuromuscular diseases, Katsuno et al., went on to measure DCTN1 mRNA levels in motorneuron cell bodies via *in situ* hybridization. They found decreased DCTN1 mRNA in the motorneuron cell bodies of AR-97Q mice compared to controls. Katsuno et al., hypothesized that nuclear accumulations of pathogenic AR protein due to the polyglutamine tract expansion were responsible for the disruption of DCTN1 expression. Indeed they were able to reverse DCTN1 *and* subsequent retrograde transport deficits via castration of male AR-97Q animals (Katsuno et al., 2006).

To further assess the functionality of transport mechanisms of motorneuron axons in our 30d and 120d Muscle[BDNF] knockout animals, we performed sciatic nerve ligation experiments based on those performed by Katsuno et al. In our study, we immunolabeled α-tubulin, synaptophysin, NF-H-P and DCTN1 in the sciatic nerve. Both synaptophysin and NF-H are bi-directionally transported via microtubule-dependent mechanisms in motorneuron axons, though NF-H-P is associated with retrograde transport only. We

labeled DCTN1 protein because deficits in DCTN1 have been seen in motorneurons in other neuromuscular disease models, including the AR-97Q animal model (Katsuno et al., 2006) (Katsuno et al.) We hypothesized that deficits in motorneuron axonal retrograde transport due to a lack of skeletal-muscle synthesized BDNF, result in decreased accumulation of synaptophysin, NF-P-H and DCTN1 proteins immediately distal to the ligation site when compared to control animals who were expected to build up significantly more of these proteins at that physical barrier in the sciatic nerve.

Methods

Sciatic Nerve Ligation

The following methods are based on the ligation experiments performed by Katsuno et al., (Katsuno et al., 2006).

Two hours prior to surgery, 30d and 120d animals were given 2.5mg/kg of the nonsteroidal anti-inflammatory drug (NSAID; meloxicam; Boehringer Ingelheim Vetmedica, Inc., Ingelheim am Reihn, Germany). One hour prior to surgery, animals were given another 2.5mg/kg of meloxicam and 2.5mg/kg of buprenorphine (Hospira, Inc., Lake Forest, IL) as an analgesic. Animals were anesthetized using Isofluorane (Henry Schein Animal Health) and a small incision was made in the skin at mid-thigh level. Next, the sciatic nerve was exposed and tied tight with silk surgical suture. The skin was closed using a 7mm wound clip, and iodine was applied. Animals were monitored every hour for signs of distress. Four hours post-surgery, another dose (2.5mg/kg) of buprenorphine was administered as a supplemental analgesic. Eight hours

after ligation, animals were euthanized via I.P. injection of the sodium pentobarbital

solution Beuthanasia-D (Schering Plough Animal Health). Cardiac perfusion was

performed using 0.9% saline, followed by 4% paraformaldehyde. Once the ligated nerve

was re-exposed, an additional piece of suture, which would remain attached until nerve

was frozen in OCT, was tied approximately 1cm distal to the ligation site to avoid

confusing the orientation once the segment of nerve was removed and floating in fixative.

The sciatic nerve was removed so that there was at least 0.5cm of tissue both distal and

proximal to the ligation site. The sciatic nerve was placed in paraformaldehyde (4% in

1:9 0.2M monobasic:0.2M dibasic sodium phosphate buffer, pH 7.4) for 1hr, then

transferred to 20% sucrose (in 1:9 0.2M monobasic;0.2 dibasic sodium phosphate buffer,

pH 7.4) for 24hr or until equilibrated.

Tissue Sectioning and Immunohistochemistry

The silk suture was carefully removed from the ligation site and the sciatic nerve

tissue was placed in a plastic tissue mold, being mindful of proximal and distal

orientation, covered with OCT and frozen with dry ice. The frozen tissue was sectioned

longitudinally at 14µm onto gelatin-coated slides. 30d and 120d tissue was chemically

crosslinked to gelatin-coated slides by incubating for 20 min in paraformaldehyde (4% in

1:9 0.2M monobasic:0.2M dibasic sodium phosphate buffer, pH 7.4), then rinsed with

1XPBS (14mM sodium chloride, 2.7mM potassium chloride, 1.5mM monobasic

potassium phosphate, 8.0mM dibasic sodium phosphate heptahydrate, pH 7.4). 30d and

120d tissue was next incubated in blocking buffer (10% normal donkey serum, 0.2%

Triton X-100 and 0.01% sodium azide in 1XPBS) for 1hr. 30d and 120d tissue was then

incubated for 24hr at room temp and an additional 24hr at 4°C with the following

primary antibodies in blocking buffer: anti-NF-H-P 1:1000 (Covance), anti-

synaptophysin 1:500 (Abcam), anti-DCTN1 1:200 (Santa-Cruz), and anti-α-tubulin 1:200

(Abcam). Primaries were rinsed with 1X PBS and tissue was incubated with the

following secondary antibodies (with 0.2% Triton X-100 in 1XPBS) for 1hr: Alexa-405-

conjugated donkey anti-chicken, Alexa-488-conjugated donkey anti-mouse, Alexa-594-

conjugated donkey anti-goat, and Alexa-647-conjugated donkey anti-rabbit (all 1:200;

Jackson Labs). Slides were rinsed with 1X PBS, air-dried 4-6hrs, and coverslipped with

ProLong gold anti-fade mounting media (Life Technologies).

Imaging and data collection

Using an Olympus Fluoview FV1000 confocal laser scanning microscope, 20

images total per animal were acquired: 10 images of the segment of sciatic nerve

immediately proximal to ligation site, and 10 images of the segment immediately distal.

See Figure X for an example of these images. Scanning speed, aspect ratio, digital zoom,

and step size were set at 20μs/pixel, 1040 X 1040, 1.6, and 4.77μm respectively.

Confocal images were uploaded into IMARIS 3D rendering software (Bitplane) for data

collection. Separate surfaces were created for each protein (synaptophysin, NF-H-P, and

DCTN1) within 500 μm of the ligation site (see Figure 8 for example). Total surface area

for each surface was obtained and one-way ANOVA and Bonferroni post-test statistical

analyses were performed, using GraphPad Prism software, to determine the accumulation

of synaptophysin, NF-H-P, and DCTN1 on the distal and proximal sides of the ligation

site in experimental and control animals at both time points.
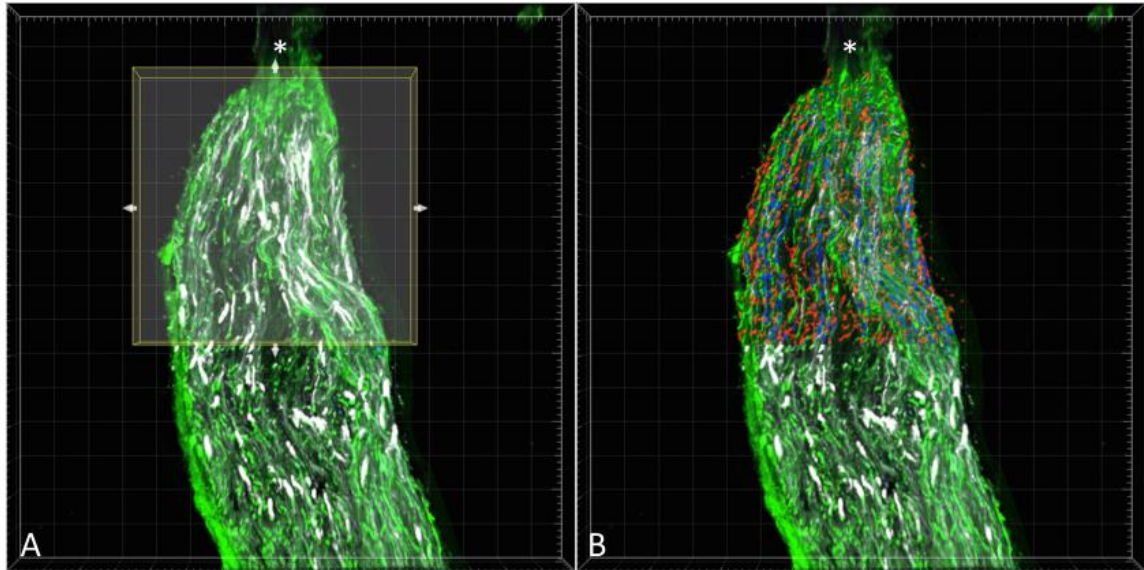
Figure 20. 3D rendering of segment of sciatic nerve immediately distal to ligation site using IMARIS. 500μm of this distal sciatic nerve segment was measured (A) from ligation site (*) and 3D surface renderings were created within that distance (B) for α-tubulin (blue), NF-H-P (green), DCTN1 (red), and synaptophysin (gray).

Results

To assess potential disruptions in retrograde transport in 30d and 120d Muscle[BDNF] deficient mice, sciatic nerve ligation was performed and the amount of synaptophysin, NF-H-P and DCTN1 accumulated distal to the ligation site was measured. Accumulation of the same proteins proximal to the ligation site was also measured and compared across genotypes to determine if there were deficits in anterograde transport.

At 120d, there was a significant decrease in immunoreactivities of NF-H-P and DCTN1 in the distal sciatic nerve in Muscle[BDNF-/-] animals only (p<0.01) (Figures 21B and 22). There were no significant differences in accumulation of synaptophysin in the

distal sciatic nerve across genotypes (Figure 23B). In the proximal portion of the nerve, there were no significant differences between Muscle[BDNF] deficient or control animals in terms of NF-H-P or synaptophysin (Figures 21B and 23B). There was a significant increase in DCTN1 accumulation at the proximal site in both Muscle[BDNF-/-] and Muscle[BDNF+/-] 120d mice ($p<0.05$) (Figure 22).

At 30d, preliminary data shows that there is no significant change in mean NF-H-P or synaptophysin immunofluorescence accumulated distal to the ligation site (Figures 21A and 23A). While there seems to be a trend indicating an increase in accumulation of both of these proteins distal to the ligation site, this trend does not reach significance (Figures 21A and 23A).
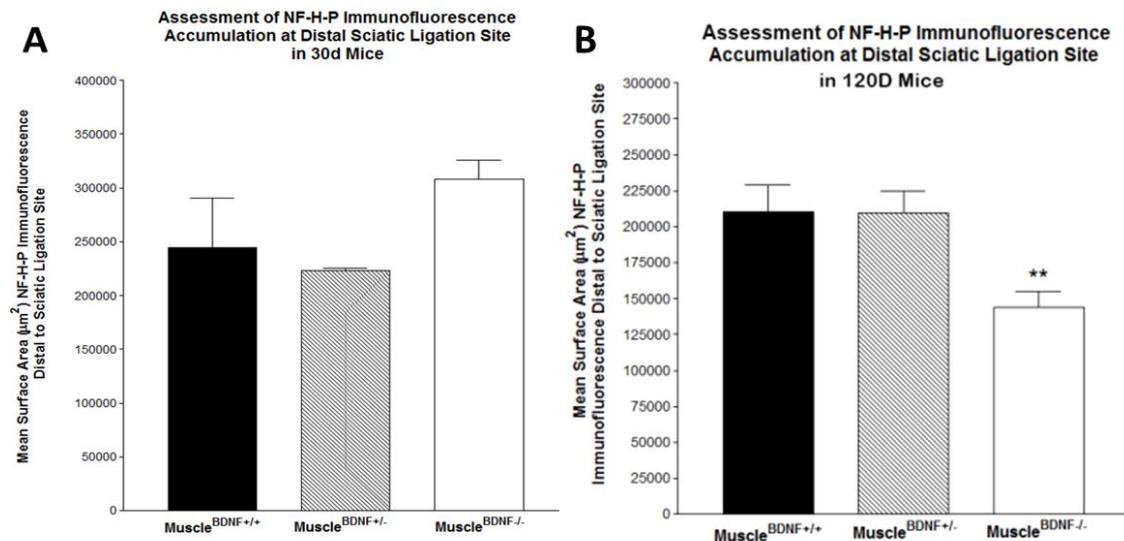
Figure 21. Mean surface area of NF-H-P immunofluorescence immediately distal to ligation site in 30d and 120d animals. At 30d, there is no significant change in mean surface area of NF-H-P immunofluorescence across genotypes (A)(n=5 animals per genotype). At 120d, mean surface area of NF-H-P immunofluorescence is significantly decreased in Muscle[BDNF-/-] animals compared to controls ($p<0.01$), while that of Muscle[BDNF+/-] animals does not change (B) (n=7 animals per genotype).

Assessment of Dynactin Immunofluorescence Accumulation at Distal Sciatic Ligation Site
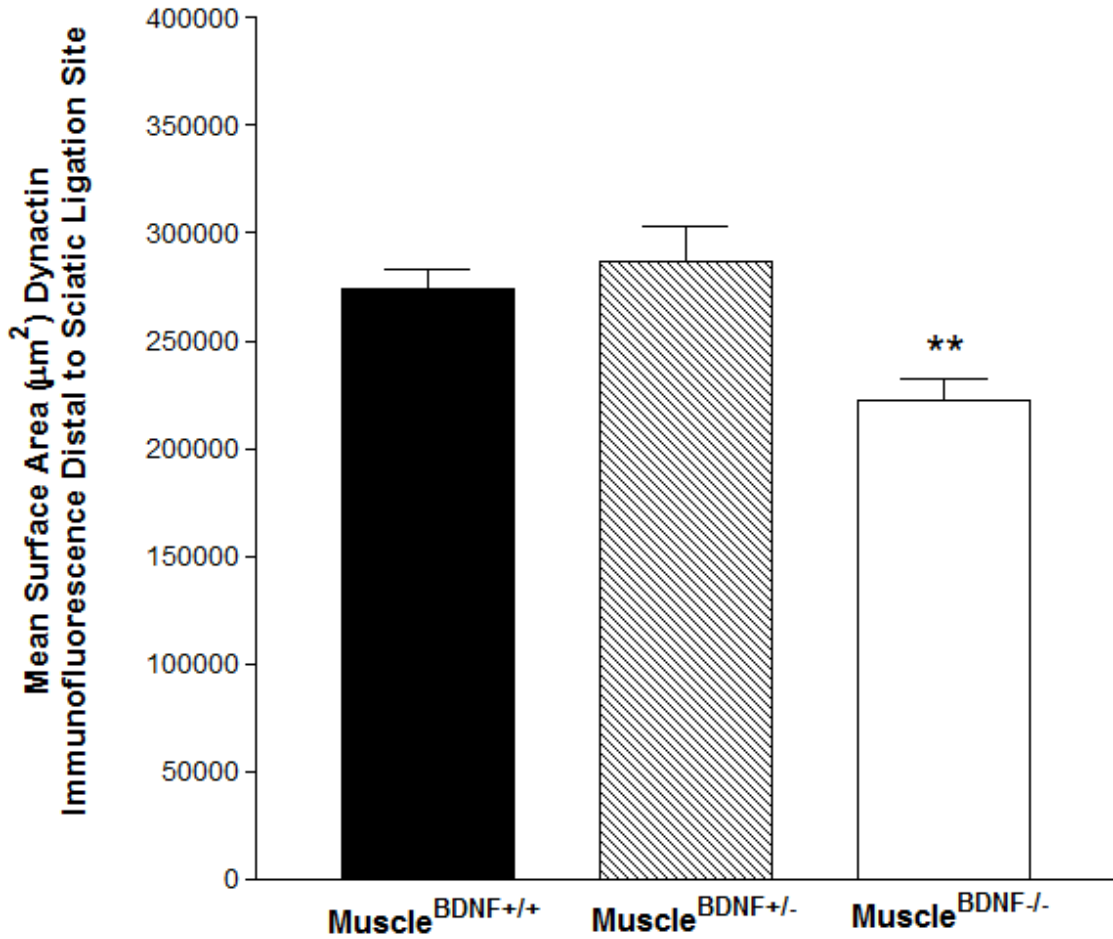
Figure 22. Mean surface area of DCTN1 immunofluorescence immediately distal to ligation site in 120d animals. Mean surface area of DCTN1 immunofluorescence is significantly decreased in Muscle[BDNF-/-] animals compared to controls (p<0.01), while that of Muscle[BDNF+/-] animals does not change. (n=7 animals per genotype)

A Assessment of NF-H-P Immunofluorescence Accumulation at Distal Sciatic Ligation Site in 30d Mice

B Assessment of NF-H-P Immunofluorescence Accumulation at Distal Sciatic Ligation Site in 120D Mice
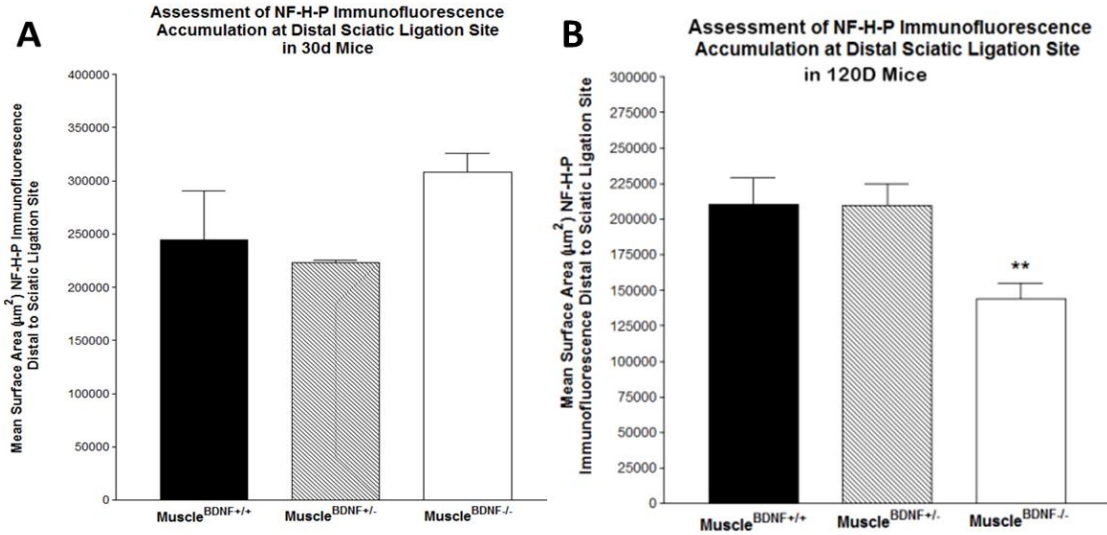
Figure 23. Mean surface area of synaptophysin immunofluorescence immediately distal to ligation site in 30d and 120d animals. At 30d, there is no significant change in mean surface area of synaptophysin immunofluorescence across genotypes (A) (n=5 animals per genotype). At 120d, mean surface area of synaptophysin immunofluorescence does not change across genotypes (B) (n=7 animals per genotype).

Assessment of NF-H-P Immunofluorescence Accumulation at Proximal Sciatic Ligation Site
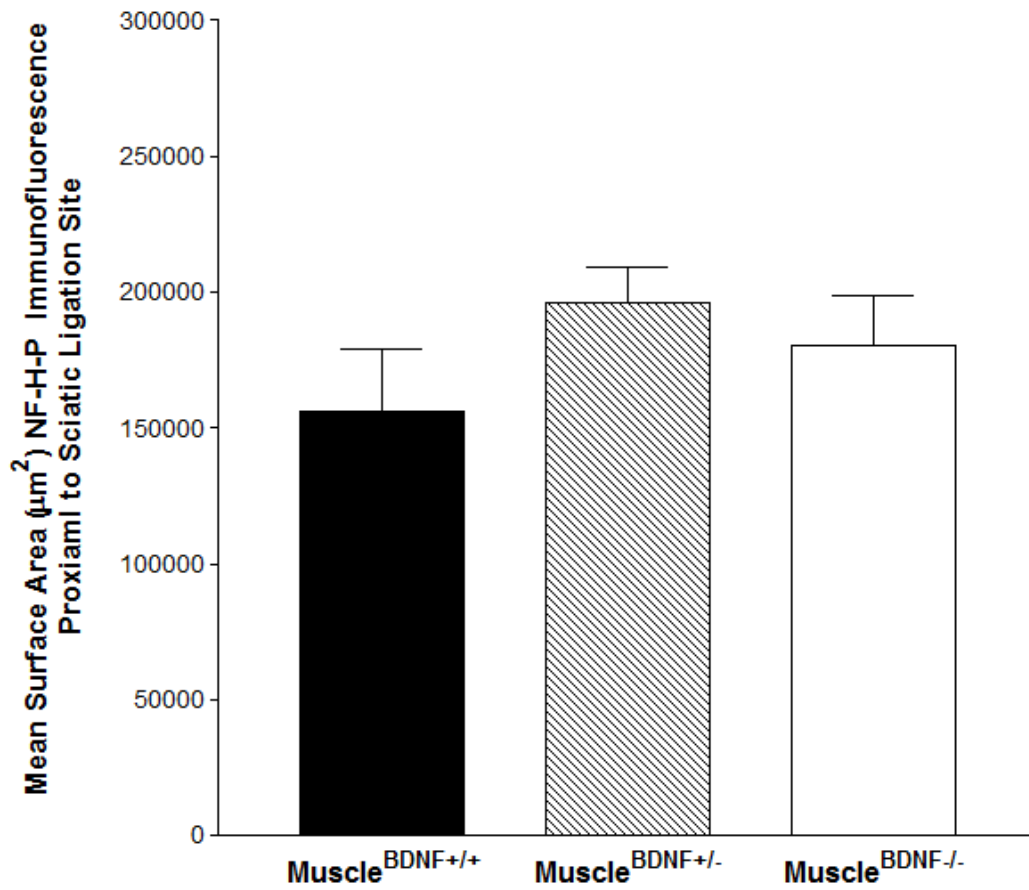
Figure 24. Mean surface area of NF-H-P immunofluorescence immediately proximal to ligation site in 120d animals. Mean surface area of NF-H-P immunofluorescence does not change across genotypes. (n=7 animals per genotype).

Assessment of Dynactin Immunofluorescence Accumulation at Proximal Sciatic Ligation Site
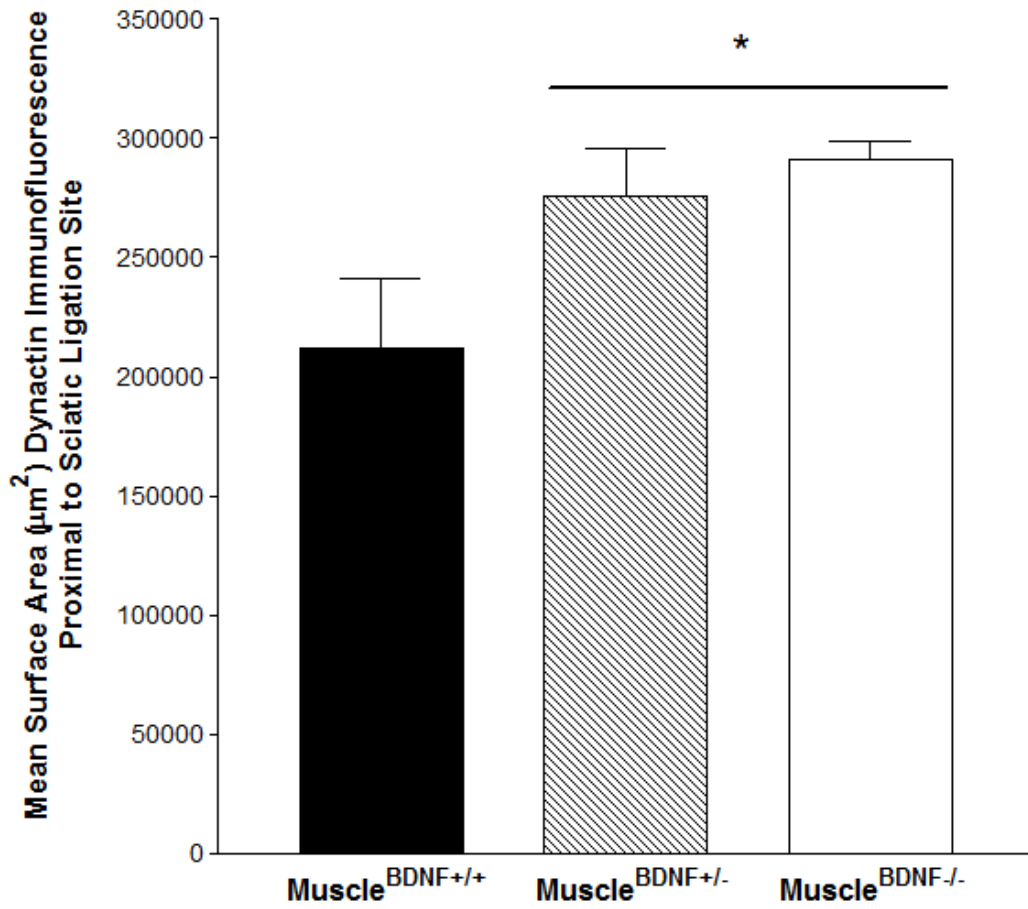
Figure 25. Mean surface area of DCTN1 immunofluorescence immediately proximal to ligation site in 120d animals. Mean surface area of DCTN1 immunofluorescence is significantly increased in Muscle[BDNF-/-] and Muscle[BDNF+/-] animals (p<0.05). (n=7 animals per genotype)

Assessment of SYN Immunofluorescence Accumulation at Proximal Sciatic Ligation Site
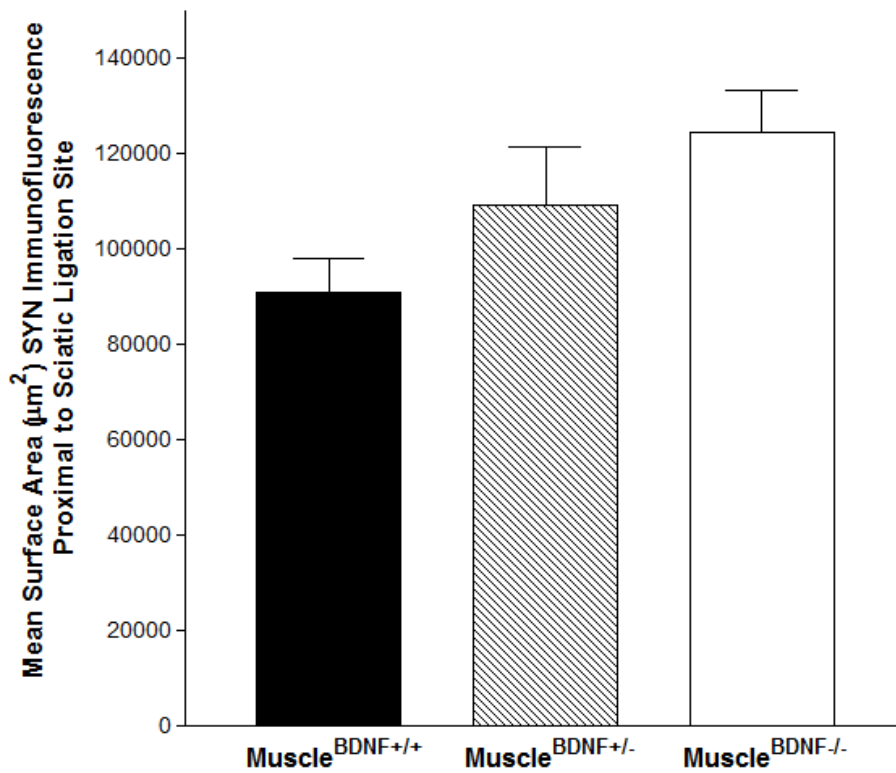
Figure 26. Mean surface area of synaptophysin immunofluorescence immediately proximal to ligation site in 120d animals. There is no significant change in synaptophysin immunofluorescence proximal to ligation site across genotypes. (n=7 animals per genotype).

Discussion

At 30d, there was no significant change in accumulation of NF-H-P or synaptophysin at the distal ligation site across genotypes (Figures 21A and 23A respectively). In the last chapter we saw that at 30d, there was no significant accumulation of NF-H-P in gastroc-associated motorneuron axon terminals in homozygous or heterozygous knockouts (Chapter 3, Figure 19A). Together these data suggest that there are no deficits in retrograde transport at 30d. This is interesting,

because we do see a significant decrease in dendritic length in heterozygous and homozygous knockouts at 30d (Chapter 1, Figure 11), which we hypothesized was actually attributed to decreased retrograde transport of the Fluorogold tracer used to visualize the motorneurons. It is possible that retrograde transport is disrupted in 30d Muscle^{BDNF} deficient animals, and that upregulation of BDNF at the motorneuron soma is sufficiently compensating for the transport of NF-H-P and synaptophysin. Previous data does show that BDNF immunofluorescence is significantly increased at the cell soma of gastroc-associated motorneurons (Chapter 1, Figure 8). It's possible that, at 30d, preliminary deficits in Fluorogold transport combined with deficits in Fluorogold internalization is enough to account for the significant decrease in dendritic length labeling that we see at 30d. We know that BDNF-TrkB signaling is involved in initiating endocytosis, and activating dynamin which pinches off the endocytotic vesicle from the presynaptic membrane (Cosker and Segal, 2014). Decreases in BDNF-TrkB regulated endocytosis in Muscle^{BDNF} deficient mice could account for decreased endocytosis of Fluorogold, and thus decreased Fluorogold labeling at the dendrites. We need to collect data for the distal accumulation of DCTN1 and the proximal accumulation of synaptophysin, NF-H-P and DCTN1 to gain a better understanding of axonal transport at 30d.

At 120d, we show significant decreases in NF-H-P and DCTN1 accumulation at the distal ligation site in Muscle$^{BDNF-/-}$ animals (Figures 21 and 22). This is consistent with data from the previous chapter showing a significant accumulation of NF-H-P in the distal axon (Chapter 3, Figure 19B). Together these data provide strong evidence that retrograde transport is disrupted in 120d homozygous knockouts, and that skeletal

muscle-synthesized BDNF-TrkB interactions are required for normal retrograde transport at 120d.

In 120d heterozygous knockouts, there is no significant change in NF-H-P or DCTN1 accumulation levels at the distal ligation site (Figures 21B and 22). However, we did see significant accumulation of NF-H-P in the distal gastroc-associated axons in this genotype at 120d (Chapter 3, Figure 19B). Previous data shows that BDNF immunofluorescence at the motorneuron soma is significantly increased in 120d Muscle$^{BDNF+/-}$ animals (Chapter 1, Figure 8). The increase in BDNF synthesis at the soma could lead to increased expression and anterograde transport of DCTN1 in an attempt to compensate for deficiencies in retrograde transport. Additionally, it is possible that BDNF is being anterogradely transported and secreted at the axon terminal in order to act as an autocrine signaling molecule to initiate BDNF-TrkB dependent signaling cascades that are responsible for the assembly of DCTN1/dynein-cargo complexes. An increase in DCTN1 at the proximal ligation site in Muscle$^{BDNF+/-}$ animals would lend support to this model.

Indeed, at 120d, we show that there is a significant increase in DCTN1 at the proximal ligation site in both heterozygous and homozygous knockout animals (Figure 25). While compensatory mechanisms seem to be sufficient for ameliorating the retrograde transport of NF-H-P and DCTN1 in the heterozygous knockouts, it is still not enough to maintain retrograde transport of these proteins in our homozygous knockouts.

At 120d, there were no significant differences in synaptophysin accumulation either distal or proximal to the ligation site across genotypes (Figures 23 and 26). It is possible that an increase in DCTN1 synthesized and transported throughout the axon to

51

aid in recycling as described above maintains proper vesicular transport in heterozygous knockouts. We expected to see a significant decrease in synaptophysin accumulated distal to the ligation site as a result of disrupted retrograde transport. Our laboratory has shown that the presynapse has a decreased surface area in animals lacking skeletal muscle-synthesized BDNF (Chapter 1, Figure 5A; Dangremond et al., 2015). We have also shown that the neuromuscular junctions are significantly fragmented in animals lacking this source of BDNF (Chapter 1, Figure 7). It is possible that synaptophysin is being upregulated at the soma to compensate for loss at the neuromuscular junction. However, if this were the case we would likely see greater accumulation of synaptophysin proximal to the ligation site as this vesicle-associated protein is bi-directionally transported. It is more likely that there is an increase in synaptophysin recycling at the presynapse as the presynaptic bouton is degenerating. This would account for the fact that while retrograde transport is disrupted, there is simply more synaptophysin being shipped to the soma compared to the amount of synaptophysin being retrogradely trafficked in control animals. Synaptophysin is regulated by the ubiquitin-proteasome system (UPS) in which ubiquitinated proteins are marked for degradation by an enzyme complex known as the proteasome (Bingol and Schuman, 2005). The ubiquitination of synaptophysin is mediated by the ubiquitin ligase Siah1 (Waites et al., 2013). Siah1 is negatively regulated by the presynaptic protein Bassoon, meaning that in the presence of Bassoon, Siah1 does not add ubiquitin to synaptophysin (Waites et al., 2013). Interestingly, Nishimune et al., show that Bassoon levels impaired by aging are actually improved by exercising (Nishimune et al., 2012). We know that BDNF is secreted from skeletal muscle during exercise, and that BDNF from skeletal muscle

modulates several key processes in motorneuron maintenance. It is not a great leap then to hypothesize that BDNF likely regulates Bassoon. In fact, BDNF levels were significantly increased in hippocampal neurons of Bassoon mutants (Heyden et al., 2011). In our homozygous Muscle$^{BDNF-/-}$ knockouts, absence of skeletal muscle-synthesized BDNF may lead to a decrease in Bassoon, which in turn would lead to more activated Siah1 and thus more ubiquitinated synaptophysin. Retrograde delivery of additional ubiquitinated synaptophysin could therefore account for the amount of synaptophysin we see accumulated distal to the ligation site in our 120d homozygous animals compared to controls. See Figure 27 for a depiction of the suggested model. Future studies should investigate the regulation of Bassoon in skeletal muscle-synthesized BDNF knockouts versus wildtype animals.
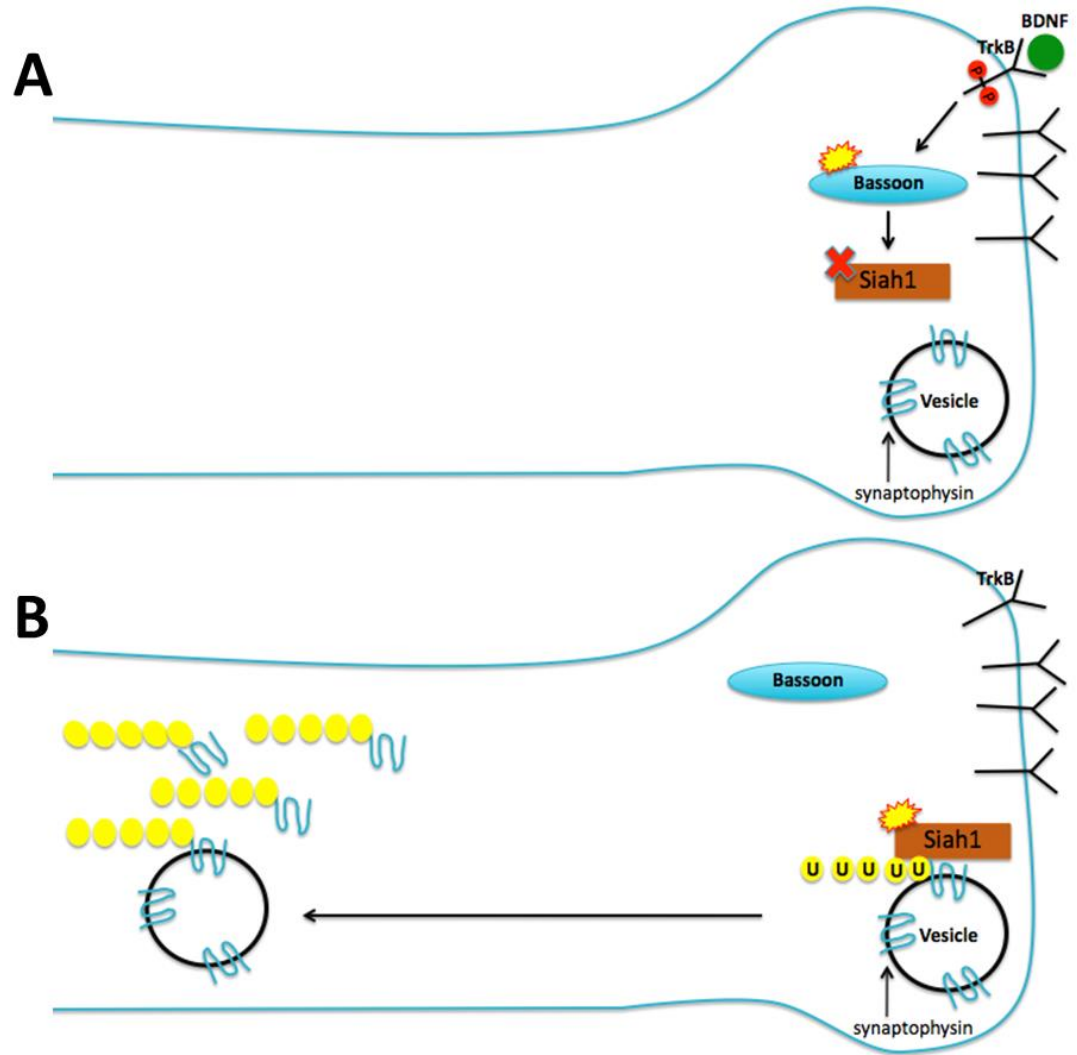
Figure 27. Skeletal muscle-synthesized BDNF indirectly regulates the ubiquitination of synaptophysin via Bassoon and Siah1. In this model, when skeletal muscle-synthesized BDNF binds to TrkB (A) at the axon terminal of an innervating motorneuron, TrkB autophosphorylates and BDNF/TrkB signaling results in the activation (yellow star) of the synaptic protein, Bassoon. Activated Bassoon inhibits the synaptophysin-ligase, Siah1 (red X). In the absence of skeletal muscle-synthesized BDNF (B), Bassoon is not activated and active Siah1 ubiquitinates synaptophysin. Ubiquitinated synaptophysin is then transported retrogradely to the cell body for recycling.

An alternative model, which does not necessarily negate the model described above, could be explained by recent evidence challenging the slow/fast axonal transport paradigm. We have generally accepted in recent years that there are two types of retrograde axonal transport, fast and slow. However, Lee and Mitchell, make a strong

case for an alternative in which the speed of retrograde axonal transport is represented by a large spectrum of speeds dependent on number of dynein motor proteins bound to the cargo, and the size of the cargo itself (Lee and Mitchell, 2015).   According to this model NF-H, a relatively small molecular cargo, would only require one dynein motor while a vesicle would require tens of motors. The motor/s would be able to take long "steps" with a small cargo like NF-H while taking smaller but collectively more steps while transporting a vesicle. A reduction in dynein recruitment to presynaptic cargos (mediated by BDNF) as well as reduced DCTN1 (as suggested by Figure 24) would then have a greater effect on the transport of NF-H-P versus vesicle-associated synaptophysin as taking one motor from a NF-H-P could halt the movement of that cargo while taking one motor from synaptophysin would only slow it down minutely. It's possible that an 8hr ligation was too short to be able to see differences in synaptophysin.

Thus far in our particular model, we have observed a significant accumulation of NF-H-P in distal motorneuron axons of BDNF deficient animals. We also see that NF-H-P and DCTN1 accumulation distal to ligation site is significantly lower in homozygous Muscle$^{BDNF-/-}$knockout mice. Together, these results demonstrate that there is disruption in retrograde transport.

To gain a better understanding of axonal transport dynamics in mice lacking skeletal-muscle synthesized BDNF, more experiments must be performed. One potentially enlightening experiment would be to inject the retrograde tracer Fluorogold into the gastroc muscle perform a sciatic nerve ligation in the same leg, and then measure the accumulation of Fluorogold distal to the ligation site. An advantage of this approach would be gaining a better understanding of vesicular trafficking along the axon. One of

55

the difficulties involved however would be determining the proper time-point of ligation, and how long the animals should remain alive after ligation in order to have sufficient accumulation for measurements. Because the sciatic nerve is a mixed nerve, containing sensory and motorneurons, it may also be beneficial to differentiate the neuron types to gain a better understanding of what is going on specifically in the motorneurons. *In situ* hybridization experiments in the motorneuron cell soma labeling NF-H-P, DCTN1 and synaptophysin RNA would also be helpful in understanding if expression of these genes is being upregulated to compensate for decreased or loss of skeletal muscle-synthesized BDNF. It would also be interesting to investigate the UPS at the presynapse, and measure levels of Bassoon and Siah1 gene and protein expression. It will also be important to show that retrograde transport the TrkB-BDNF signaling endosome specifically is disrupted. A ligation experiment labeling TrkB could help answer these questions.

CHAPTER FIVE: ASSESSING ROLE OF SKELETAL MUSCLE-SYNTHESIZED BDNF IN THE MAINTENANCE OF MITOCHONDRIAL DENSITY AT THE NEUROMUSCULAR JUNCTION

Introduction

We assessed mitochondrial densities at neuromuscular junctions in our skeletal muscle-synthesized BDNF deficient mice for multiple reasons. First, deficits in mitochondrial trafficking are noted in several neuromuscular diseases including ALS, HD and SBMA. Also, because of the high energy and calcium buffering demand at the presynapse, disruptions in mitochondrial transport could be detrimental to motorneurons (Chang and Reynolds, 2006; Magrané et al., 2009; de Moura et al., 2010; Nguyen et al., 1997; Orr et al., 2008; Palay, 1956; Piccioni et al., 2002; Su et al., 2010; Vos et al., 2007). Further, the PI3K and PLCγ pathways activated by BDNF binding to TrkB is required for mitochondrial docking at the presynapse (Su et al., 2014). We reasoned that the partial reduction of BDNF-TrkB binding at the presynaptic membrane in our heterozygous knockouts, or complete absence of it in our homozygous knockouts could lead to decreased mitochondrial docking at the presynapse. Finally, while studying processes related to heart failure, Takada et al., showed that skeletal muscle-synthesized BDNF maintains exercise capacity and mitochondrial function in skeletal muscle (Takada et al., 2014). The transgenic mice used in the Takeda et al., study were about 120d and were global heterozygous BDNF knockouts. Takada et al., found that phosphorylation of TrkB, BDNF binding TrkB, mitochondrial complex I and III activities were significantly reduced in these heterozygous BDNF knockouts. Phosphorylation of 5' AMP-activated protein kinase and PGC1 α were also significantly reduced in the knockout animals

compared to wildtypes (Takada et al., 2014). Takada et al., did not investigate the role of skeletal muscle-synthesized BDNF, specifically, in the maintenance - of mitochondrial function in motorneurons, but it is likely a global knockdown of BDNF also affected the neurotrophin produced in the skeletal muscle, which subsequently had an adverse effect maintaining mitochondrial function in TrkB-containing motorneurons as well.

We hypothesized that there would be a significant change in mitochondrial density at the neuromuscular junction in animals with decreased skeletal muscle-synthesized BDNF due to a combination of axonal trafficking and BDNF-TrkB signaling deficits. To label mitochondria at the neuromuscular junction, we used the fluorescent probe MitoTracker™CMXRos (Life Technologies) which is sequestered by live mitochondria. Because sequestration of the probe requires live mitochondria, the dye is almost exclusively used *in vitro*. Martin et al., recently developed a protocol in which the MitoTracker dye is injected into the gastroc of living mice, and subsequently becomes endocytosed and retrogradely transported in gastroc-associated motorneurons (Martin et al., 2007, 2009). Four days after MitoTracker injection, Martin et al., (2009) removed and sectioned the spinal cord and visualized MitoTracker in gastroc-associated motorneuron cell bodies. We adapted these procedures to visualize MitoTracker labeling at the neuromuscular junction, and also label presynaptic and postsynaptic proteins via immunohistochemistry techniques post fixation. We were successful in visualizing MitoTracker, vesicular acetyl choline transporter (VAChT; presynaptic marker), acetyl choline receptors (via α-bungarotoxin; post-synaptic marker), NF-H (innervating motorneuron) and muscle cell nuclei (via DAPI) in skeletal muscle sections of 120d control, Muscle$^{BDNF+/-}$, and Muscle$^{BDNF-/-}$ mice. Using IMARIS image analysis software,

58

we were able to measure the colocalization of MitoTracker with either VAChT or α-bungarotoxin to obtain presynaptic and postsynaptic densities respectively. VAChT was used in place of synaptophysin because we reasoned that VAChT would more efficiently delineate the presynapse, because synaptophysin labeling was often found in the axons. By using VAChT we did not have to perform subjective cropping of the IMARIS-created surface.

Methods

Injection of MitoTracker and tissue harvest

The following methods are adapted from Martin et al., (Martin et al., 2009). Stock solution of MitoTracker™ CMXRos (Life Technologies-Molecular Probes) was prepared by dissolving MitoTracker powder in DMSO to a final concentration of 1mM. The stock solution was then diluted with 0.9% saline to a final working concentration of 200nM. While studies have shown that 0.5%-1.5% DMSO can be neurotoxic, it is unlikely that the dilution we used (1.06×10^{-5}% DMSO) had any effect upon the gastroc-associated neurons. The analgesic Buprenorphine (Hospira, Inc.) was administered to animals 30min prior to injections. Animals were anesthetized using Isofluorane (Henry Schein Animal Health) and a small incision was made in the skin over the right gastroc. 6μl of 200nM MitoTracker were injected into the gastroc via 3 injections, 2μl each, proximal, medial, and distal. Skin was closed using a 7mm wound clip, and swabbed with iodine. Three days after injection of MitoTracker, animals were anesthetized and the injected gastroc was removed. The muscle was placed in a plastic tissue mold,

covered in OCT compound and frozen on dry ice. The animals were euthanized via I.P. injection of sodium pentobarbital solution Beuthanasia-D (Schering Plough Animal Health).

Tissue sectioning and immunohistochemistry

All procedures were performed in the dark due to the light sensitivity of MitoTracker. Frozen muscle was sectioned longitudinally at 40μm onto gelatin-coated slides. Sections were fixed to slides via 15min incubation with paraformaldehyde (4% in 1:9 0.2M monobasic:0.2M dibasic sodium phosphate buffer, pH 7.4). Tissue was rinsed with 1XPBS (14mM sodium chloride, 2.7mM potassium chloride, 1.5mM monobasic potassium phosphate, 8.0mM dibasic sodium phosphate heptahydrate, pH 7.4) 3 times for 5 minutes each. Tissue was incubated with blocking buffer (10% normal donkey serum, 0.2% Triton X-100, and 0.01% sodium azide in 1XPBS) and then incubated overnight with the following primary antibodies in blocking buffer: anti-NF-H 1:1000 (Millipore) and anti-VAChT 1:200 (Santa Cruz Biotechnology). Primary antibodies were rinsed off with 1XPBS and tissue was incubated for 1hr with 488-conjugated-α-bungarotoxin (Life Technologies) and the following secondary antibodies: Alexa-405-conjugated donkey anti-chicken and Alexa-647-conjugated donkey anti-goat (each 1:200; Jackson Labs) in 1XPBS solution containing 0.2% Triton X-100. Excess secondary antibodies were removed with 1XPBS washes (3X for 5minutes) and the tissue was allowed to dry. Slides were coverslipped with Vectashield containing DAPI (Vector Labs) to prevent fading of fluorophores.

15 neuromuscular junctions per animal were imaged using an Olympus Fluoview FV1000 confocal laser scanning microscope. Scanning speed, aspect ratio, digital zoom and step size were 20μs/pixel, 1024x1024, 2.5 and 4.77μ respectively. Images were rendered using IMARIS image analysis software. In IMARIS, surfaces were created for the pre- and post-synaptic and mitochondrial markers (VAChT, 488-conjugated α-bungarotoxin and MitoTracker CMXRos respectively; see Figure 28 for example. Two additional surfaces were then created representing (1) the colocalization of VAChT and MitoTracker and (2) the colocalization of α-bungarotoxin and MitoTracker (see Figure 16 for example). Total number of volumetric pixels (voxels) was measured for the colocalization surfaces as a representation of mitochondrial density at each the pre- and post-synaptic surfaces and these measurements were compared across genotypes via one-way ANOVA and Bonferroni post-test statistics, using GraphPad Prism sofware.
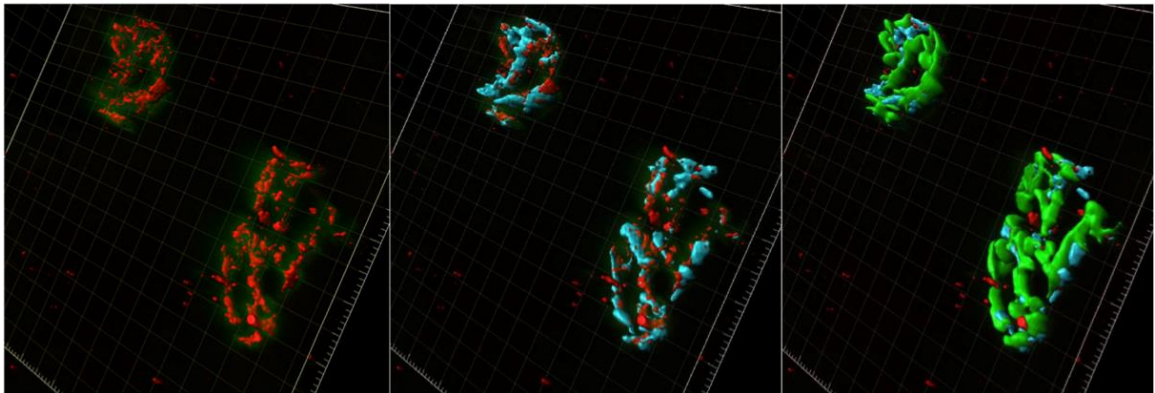
Figure 28. 3D rendering of presynaptic, postsynaptic and MitoTracker labels using IMARIS. This image shows the MitoTracker CMXRos channel rendered in red, the pre-synaptic VAChT channel in cyan and the post-synaptic α-bungarotoxin channel in green. After rendering each channel in IMARIS, additional colocalization surfaces were created representing the colocalization of MitoTracker with VAChT or colocalization of MitoTracker with α-bungarotoxin (shown in next figure). The colocalization measurements were used to compare mitochondrial density at pre- and post-synapse in skeletal muscle-synthesized BDNF knockout animals.

Results

We assessed mitochondrial density at the pre- and post-synapse in gastroc-associated NMJs. We measured the number of voxels that overlapped for MitoTracker/VAChT and MitoTracker/α-bungarotoxin. There was a significant decrease in overlapping voxels at the pre-synapse (MitoTracker/VAChT) in Muscle[BDNF-/-] mice (p<0.01), while there were no significant findings at the post-synapse (Figure 30). Figure 29 depicts a representative photomicrograph of MitoTracker-VAChT colocalization in control and Muscle[BDNF-/-] 120d animals.
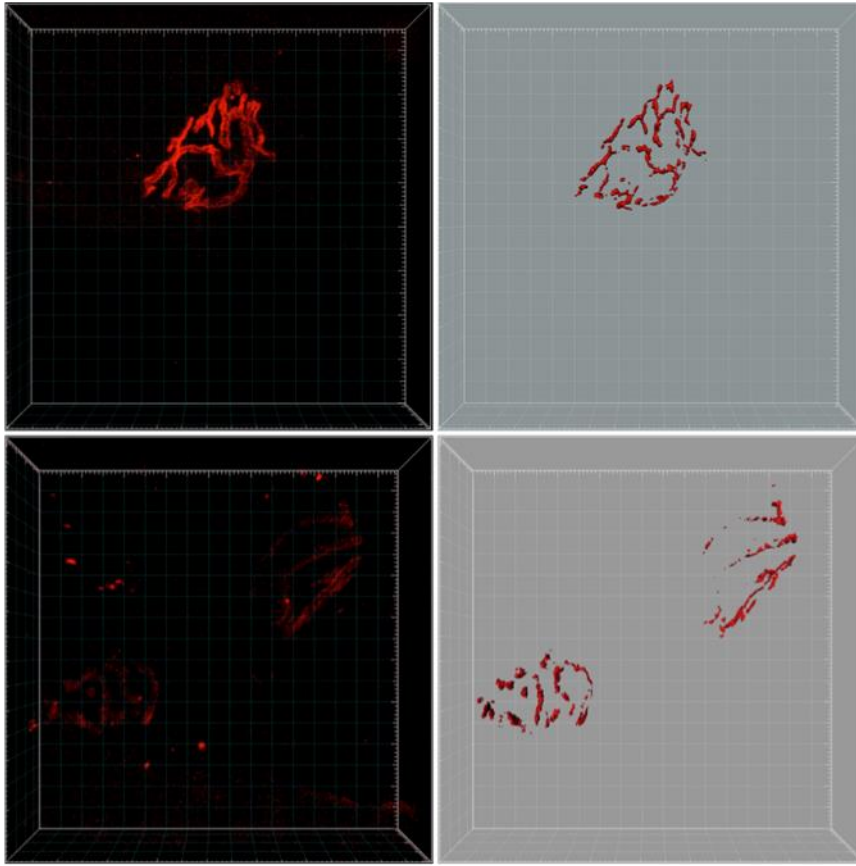
Figure 29. Representative photomicrographs showing MitoTracker colocalization with presynaptic VAChT in animals lacking skeletal muscle-synthesized BDNF

Mean voxels of MitoTracker CMXRos immunofluorescence colocalizing with presynaptic VAChT. This figure shows and example of a MitoTracker labeling at a neuromuscular junction (left) and corresponding surfaces created using IMARIS based on the colocalization of MitoTracker and the pre-synaptic marker VAChT (right) in a Muscle$^{BDNF+/+}$ control animal (top row) and Muscle$^{BDNF-/-}$ animal (bottom row).

A Mitochondrial Density in Presynaptic Boutons of the Gastroc Neuromuscular Junction

B Mitochondrial Density in Postsynaptic Muscle of the Gastroc Neuromuscular Junction
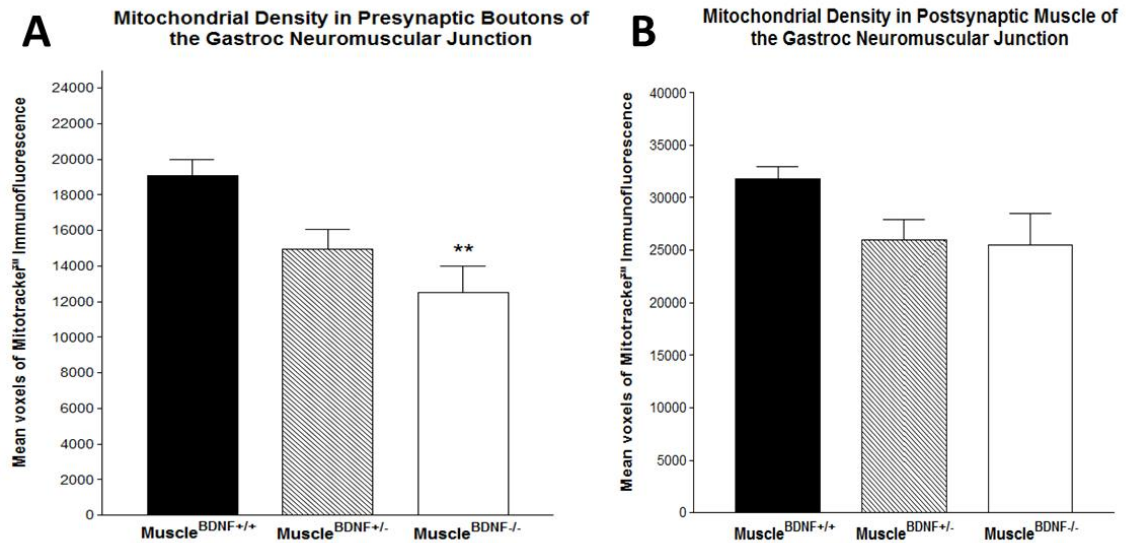
Figure 30. Mean voxels of MitoTracker Immunofluorescence colocalization with presynaptic VAChT or postsynaptic AChRs. At 120d, there is a significant decrease in mean MitoTracker-VAChT colocalization at the presynapse (A) ($p < 0.001$; n=5). There are no significant changes in MitoTracker-α-bungarotoxin colocalization at the postsynapse (B). (n=5).

Discussion

We demonstrate that MitoTracker labeling is significantly decreased in the presynaptic boutons of 120d Muscle[BDNF-/-] animals, and there is a trend showing decreased labeling in Muscle[BDNF+/-] animals (Figure 30A). There is no significant change in MitoTracker labeling at the postsynapse in our 120d knockout animals compared to controls, however we do see a trend suggesting a decrease in mitochondria at the postsynapse (Figure 30B). These results are consistent with previous data from our lab showing decreased surface area of gastroc-associated presynaptic terminals, but no change in postsynaptic area in 120d Muscle[BDNF-/-] mice (Chapter 1, Figure 5;

64

Dangremond et al., 2015). Together these data indicate that pathology in the presynapse

precedes pathology at the postsynapse in 120d Muscle$^{BDNF-/-}$ animals.

BDNF-TrkB signaling is required for recruitment of mitochondria to presynapse,

where there are high ATP-demands (Su et al., 2014). Decreased skeletal muscle-

synthesized BDNF may lead to decreased mitochondrial recruitment, and thus a decrease

in mitochondria at the presynapse. It is also possible that there are more mitochondria

present at the presynaptic terminal than we are seeing. MitoTracker is sequestered by

live mitochondria, so dead or degenerating mitochondria at the presynapse would not

sequester the dye, and thus would not be included in our analysis. Alternatively,

mitochondria at the presynapse with decreased electrochemical gradient would sequester

less MitoTracker, resulting in decreased signal. To address the potential of accumulated

dead or degenerating mitochondria at the axon terminal in knockout animals, an antibody

that binds to translocase of the outer membrane complexes in addition to MitoTracker

labeling could be used. Utilizing this method would enable both inactive and active

mitochondria to be labeled, thus providing a better picture of mitochondrial density at the

presynapse, and perhaps it would illuminate deficits in retrograde mitochondrial transport

along motorneuron axons.

Significantly decreased density of MitoTracker™CMXRos fluorescence at the

presynapse in 120d Muscle$^{BDNF-/-}$ provides a platform from which to base further studies

into motorneuron mitochondrial pathologies that are related to deficits in skeletal muscle-

synthesized BDNF. Future studies should investigate mitochondrial transport in

motorneuron axons of MuscleBDNF knockout animals. Combining MitoTracker

injection and sciatic nerve ligation techniques could illustrate mitochondrial movement

along motorneuron axons. It would also be worthwhile to investigate levels of reactive oxygen species to determine if mitochondria that are at the presynapse in Muscle[BDNF] deficient mice are healthy, or have become old and begin to passively release toxic species due to the disrupted retrograde transport we have seen thus far in this animal model. Further studies should also investigate potential mitochondrial pathologies in the skeletal muscle.

CHAPTER SIX: SUMMARY AND CONCLUSIONS

Previous findings in our laboratory indicated that there is disruption in retrograde transport along motorneuron axons in skeletal muscle-synthesized BDNF deficient mice. Pomeroy et al., (2013) showed that motorneuron dendrites labeled with the retrograde tracer Fluorogold were shorter in heterozygous and homozygous knockouts at 30d and 120d. Fluorogold was injected into the gastroc and relied on retrograde transport along the axons of gastroc-associated axons to reach and fill the soma and dendrites. The maximum motorneuron dendritic length of control animals in the study was about 250μm while the average dendritic length of lumbar motorneurons in adult mice is 2000μm. It was reasonable to assume then that the results indicated that it was likely disruptions in retrograde transport that accounted for the decrease in dendritic length values rather than an actual shortening of the dendrites. Therefore, we aimed to test the hypothesis that retrograde transport is disrupted in animals with reduced or absent skeletal muscle-synthesized BDNF.

We show that there are clear deficits in retrograde transport of NF-H-P in Muscle$^{BDNF-/-}$ animals at 120d. In these animals, there is significant accumulation of NF-H-P in distal axons of gastroc-associated motorneurons (Chapter 3, Figure 19B). Furthermore, at this age, homozygous knockouts show decreased accumulation of the retrogradely transported NF-H-P and DCTN1 proteins distal to ligation site. There was no apparent change in synaptophysin immunofluorescence at the distal ligation site, however this can be accounted for by a decrease in BDNF-regulated Bassoon. A decrease in Bassoon would lead to increased activation of Siah1, the ligase responsible

for the ubiquitination of synaptophysin. Increased ubiquitination of synaptophysin would lead to an increase in synaptophysin being retrogradely transported for degradation by the UPS. The sheer abundance of synaptohysin being retrogradely transported could account for the amount of this protein accumulated at the distal ligation site.

Anterograde transport appears to be normal in 120d Muscle$^{BDNF-/-}$ animals, as there are no significant changes in accumulation of bi-directionally transported synaptophysin at the proximal ligation site (Figure 16). There is a significant increase in DCTN1 at the proximal ligation site in 120d homozygous knockouts. Compensatory mechanisms at the soma could account for an increase in DCTN1 delivery to the axon terminal. However, with the lack of skeletal muscle-synthesized BDNF binding to TrkB at the terminal, the assembly of DCTN1/dynein-cargo complexes is not sufficient for efficient retrograde transport.

In 120d Muscle$^{BDNF+/-}$ animals, we show a significant increase in NF-H-P in the distal axons gastroc-associated motorneurons. At the same age, these animals show no significant differences in accumulation of NF-H-P, DCTN1 or synaptophysin at the distal ligation site. It's possible that compensatory mechanisms at the motorneuron soma are responsible for sending more DCTN1 to the presynapse. This is supported by the significant increase in DCTN1 at the proximal ligation site in 120d heterozygous knockouts. Motorneuron synthesized BDNF may also be anterogradely trafficked to and secreted from the axon terminal to act as an autocrine signaling molecule on the presynaptic TrkB receptors. Motorneurons of the heterozygotes are receiving some skeletal muscle-synthesized BDNF and together with aforementioned compensatory

mechanisms this may be enough to form the necessary DCTN1/dynein-cargo interactions and maintain normal levels of retrograde transport in this genotype.

30d homozygous and heterozygous knockout animals show no significant accumulation of NF-H-P in distal axons, nor do they show changes in accumulation of NF-H-P or synaptophysin at the distal ligation site. While this data implies that there are no retrograde transport deficits at this age, we need to obtain data for DCTN1 at the distal ligation site and NF-H-P, synaptophysin and DCTN1 at the proximal site to have a better picture of transport mechanisms at this age. It is possible that retrograde transport isn't significantly affected at 30d in homozygous and heterozygous knockout animals, and that decreased BDNF-TrkB-dependent endocytosis at the presynapse accounts for a decrease in Fluorogold endocytosis in 30d gastroc-associated motorneurons (Cosker and Segal, 2014).

It will be important to assess expression levels of NF-H-P, synaptophsyin and DCTN1 at the motorneuron soma to gain a better understanding of compensatory mechanisms in Muscle$^{BDNF+/-}$ and Muscle$^{BDNF-/-}$ animals. It will also be important to assess the specific retrograde transport of BDNF-TrkB signaling endosomes along gastroc-associated motorneuron axons. Assessing Bassoon and activated Siah1 protein levels at the presynapse could help determine if there is an increase in synaptophysin degradation occurring. We could also investigate ubiquitination levels of synaptophysin, and measure the potential accumulation of polyubiquitinated synaptophysin in future ligation experiments. It will also be important to investigate the role of skeletal muscle-synthesized BDNF in endocytosis at the motorneuron presynapse in our knockout model.

When assessing mitochondrial density at the neuromuscular junction, we found that there is a significant decrease in MitoTracker-VAChT colocalization at the presynapse in 120d homozygous knockouts (Figure 30A), indicating that there is a decrease in mitochondria at the presynapse in these animals at the age. A decrease in presynaptic surface area could account for the decrease in mitochondria at the presynapse. It is also possible that there are dead or degenerative mitochondria at the presynapse that aren't being labeled by the MitoTracker dye that depends on sequestration by live mitochondria. A third explanation for the decrease in mitochondria at the presynapse is that BDNF-TrkB is required for the recruitment of mitochondria at the presynapse and with a loss of BDNF from skeletal muscle, less mitochondria are recruited (Su et al., 2014). These scenarios are not mutually exclusive. We do see a trend indicating a decrease in mitochondrial density at the postsynapse of 120d homozygous and heterozygous knockouts, though this trend does not reach significance.

Using a different mitochondrial marker at the presynapse that labels dead mitochondria as well as live could indicate whether there is an accumulation of degenerative or dead mitochondria at the presynapse due to retrograde transport deficits. It would also be useful to be able to do live-tracking of mitochondria in motorneurons of our BDNF knockout model. It will also be important to investigate the role of skeletal muscle-synthesized BDNF in mitochondrial recruitment to the presynapse using our knockout model.

We have shown significant deficits in retrograde transport and mitochondrial density in animals lacking a skeletal muscle source of BDNF. These results indicate that skeletal muscle-synthesized BDNF is necessary for normal retrograde transport in

gastroc-associated motorneurons. The results presented in this thesis provide a strong

platform from which to base further investigation into the role of skeletal muscle-

synthesized BDNF.

REFERENCES

Ackerley, S., Thornhill, P., Grierson, A.J., Brownlees, J., Anderton, B.H., Leigh, P.N., Shaw, C.E. and Miller, C.C. (2003). Neurofilament heavy chain side arm phosphorylation regulates axonal transport of neurofilaments. J. Cell Biol. *161*, 489-495.

Aloyz, R.S., Bamji, S.X., Pozniak, C.D., Toma, J.G., Atwal, J., Kaplan, D.R. and Miller, F.D. (1998). p53 is essential for developmental neuron death as regulated by the TrkA and p75 neurotrophin receptors. J. Cell Biol. *143*, 1691-1703.

Al-Shamma, H.A., and Arnold, A.P. (1995). Importance of target innervation in recovery from axotomy-induced loss of androgen receptor in rat perineal motoneurons. J. Neurobiol. *28*, 341–353.

Al-Shamma, H.A., and Arnold, A.P. (1997). Brain-derived neurotrophic factor regulates expression of androgen receptors in perineal motoneurons. PNAS *94*, 1521–1526.

Altar, C.A., Cai, N., Bliven, T., Juhasz, M., Conner, J.M., Acheson, A.L., Lindsay, R.M., and Wiegand, S.J. (1997). Anterograde transport of brain-derived neurotrophic factor and its role in the brain. Nature *389*, 856–860.

Bingol, B., and Schuman, E.M. (2005). Synaptic protein degradation by the ubiquitin protasome system. Curr. Opin. Neurobiol. *15*, 536-541.

Bisby, M.A., and Tetzlaff, W. (1992). Changes in cytoskeletal protein synthesis following axon injury and during axon regeneration. Mol Neurobiol *6*, 107–123.

Bodo, C., and Rissman, E.F. (2008). The Androgen Receptor Is Selectively Involved in Organization of Sexually Dimorphic Social Behaviors in Mice. Endocrinology *149*, 4142–4150.

Borrell-Pages, M., Canals, J.M., Cordelieres, F.P., Parker, J.A., Pineda, J.R., Grange, G., Bryson, E.A., Guillermier, M., Hirsch, E., Hantraye, P., et al. (2006). Cystamine and cysteamine increase brain levels of BDNF in Huntington disease via HSJ1b and transglutaminase. J Clin Invest *116*, 1410–1424.

Brännström, T., Havton, L., and Kellerth, J.-O. (1992). Restorative effects of reinnervation on the size and dendritic arborization patterns of axotomized cat spinal α-motoneurons. J. Comp. Neurol. *318*, 452–461.

Brunet, A., Bonni, A., Zigmond, M.J., Lin, M.Z., Juo, P., Hu, L.S., Anderson, M.J., Arden, K.C., Blenis, J. and Greenberg, M.E. (1999). Akt promotes cell survival by phosphorylating and inhibiting a Forkhead transcription factor. Cell *96*, 857-868.

Cai, Q., and Sheng, Z.-H. (2012). Mitochondrial transport in neurons: impact on synaptic homeostasis and neurodegeneration. Nature Rev Neurosci *13*, 77+.

Cassina, P., Cassina, A., Pehar, M., Castellanos, R., Gandelman, M., León, A. de, Robinson, K.M., Mason, R.P., Beckman, J.S., Barbeito, L., et al. (2008). Mitochondrial Dysfunction in SOD1G93A-Bearing Astrocytes Promotes Motor Neuron Degeneration: Prevention by Mitochondrial-Targeted Antioxidants. J. Neurosci. *28*, 4115–4122.

Catapano, L.A., Magavi, S.S. and Macklis, J.D. (2008). Neuroanatomical tracing of neuronal projections with Fluoro-Gold. Methods Mol Biol- Clifton Then Totowa *438*, 353-359.

Chang, D.T.W., and Reynolds, I.J. (2006). Mitochondrial trafficking and morphology in healthy and injured neurons. Prog Neurobiol *80*, 241–268.

Cheng, P.L., Song, A.H., Wong, Y.H., Wang, S., Zhang, X. and Poo, M.M. (2011). Self-amplifying autocrine actions of BDNF in axon development. Proc Natl Acad Sci *108,*18430-18435.

Chevalier-Larsen, E. and Holzbaur, E.L. (2006). Axonal transport and neurodegenerative disease. Biochimica et Biophysica Acta (BBA)-Molecular Basis of Disease *1762*, 1094-1108.

Cosker, K.E., and Segal, R.A. (2014). Neuronal Signaling through Endocytosis. Cold Spring Harb Perspect Biol *6*, a020669.

Dangremond, R.L., Taisto, A.E., Agee, C.M., Bosink, A.M., Froberg, T.W., Ennamany, J.E., O'Brien, E.R., Porter, T.J., Ottem, E.N. Myofiber hypertrophy, neuromuscular junction fragmentation, and retrograde transport dysfunction are all pathologies associated with mice missing muscle-synthesized BDNF. Poster presented at: Society for Neuroscience; 2015 Oct 16-21; Chicago, IL.

Datta, S.R., Dudek, H., Tao, X., Masters, S., Fu, H., Gotoh, Y. and Greenberg, M.E. (1997). Akt phosphorylation of BAD couples survival signals to the cell-intrinsic death machinery. Cell *91*, 231-241.

Dijkhuizen, P.A., and Ghosh, A. (2005). BDNF regulates primary dendrite formation in cortical neurons via the PI3-kinase and MAP kinase signaling pathways. J. Neurobiol. *62*, 278–288.

Dompierre, J.P., Godin, J.D., Charrin, B.C., Cordelières, F.P., King, S.J., Humbert, S., and Saudou, F. (2007). Histone Deacetylase 6 Inhibition Compensates for the Transport Deficit in Huntington's Disease by Increasing Tubulin Acetylation. J. Neurosci. *27*, 3571–3583.

Duncan, J.E. and Goldstein, L.S. (2006). The genetics of axonal transport and axonal transport disorders. PLoS Genet. *2*, 124.

Gazula, V.-R., Roberts, M., Luzzio, C., Jawad, A.F., and Kalb, R.G. (2004). Effects of limb exercise after spinal cord injury on motor neuron dendrite structure. J. Comp. Neurol. *476*, 130–145.

Gharami, K., Xie, Y., An, J.J., Tonegawa, S., and Xu, B. (2008). Brain-derived neurotrophic factor over-expression in the forebrain ameliorates Huntington's disease phenotypes in mice. J. Neurochem. *105*, 369–379.

Ginty, D.D., and Segal, R.A. (2002). Retrograde neurotrophin signaling: Trk-ing along the axon. Curr. Opin. Neurobiol. *12*, 268–274.

Goldstein, M.E., Sternberger, L.A. and Sternberger, N.H. (1987). Varying degrees of phosphorylation determine microheterogeneity of the heavy neurofilament polypeptide (Nf-H). J. Neuroimmunol. *14*, 135-148.

Gómez-Pinilla, F., Ying, Z., Roy, R.R., Molteni, R., and Edgerton, V.R. (2002). Voluntary Exercise Induces a BDNF-Mediated Mechanism That Promotes Neuroplasticity. J. Neurophysiol. *88*, 2187–2195.

Greenberg, M.E., Xu, B., Lu, B., and Hempstead, B.L. (2009). New Insights in the Biology of BDNF Synthesis and Release: Implications in CNS Function. J. Neurosci. *29*, 12764–12767.

He, Y., Francis, F., Myers, K.A., Yu, W., Black, M.M. and Baas, P.W. (2005). Role of cytoplasmic dynein in the axonal transport of microtubules and neurofilaments. J.Cell Biol. *168*, 697-703.

Heyden, A., Ionescu, M.C.S., Romorini, S., Kracht, B., Ghiglieri, V., Calabresi, P., Seidenbecher, C., Angenstein, F. and Gundelfinger, E.D. (2011). Hippocampal enlargement in Bassoon-mutant mice is associated with enhanced neurogenesis, reduced apoptosis, and abnormal BDNF levels. Cell Tissue Res *346*, 11-26.

Howe, C.L., and Mobley, W.C. (2005). Long-distance retrograde neurotrophic signaling. Curr. Opin. Neurobiol. *15*, 40–48.

Howells, D.W., Porritt, M.J., Wong, J.Y.F., Batchelor, P.E., Kalnins, R., Hughes, A.J., and Donnan, G.A. (2000). Reduced BDNF mRNA Expression in the Parkinson's Disease Substantia Nigra. Exp. Neurol. *166*, 127–135.

Iii, J.F.D., Dabney, L.P., Karki, S., Paschal, B.M., Holzbaur, E.L.F., and Pfister, K.K. (1996). Functional Analysis of Dynactin and Cytoplasmic Dynein in Slow Axonal Transport. J. Neurosci. *16*, 6742–6752.

Ikenaka, K., Kawai, K., Katsuno, M., Huang, Z., Jiang, Y.-M., Iguchi, Y., Kobayashi, K., Kimata, T., Waza, M., Tanaka, F., et al. (2013). dnc-1/dynactin 1 Knockdown Disrupts Transport of Autophagosomes and Induces Motor Neuron Degeneration. PLoS One *8*.

Jiang, Y.-M., Yamamoto, M., Kobayashi, Y., Yoshihara, T., Liang, Y., Terao, S., Takeuchi, H., Ishigaki, S., Katsuno, M., Adachi, H., et al. (2005). Gene expression profile of spinal motor neurons in sporadic amyotrophic lateral sclerosis. Ann Neurol. *57*, 236–251.

Kamal, A., and Goldstein, L.S.B. (2002). Principles of cargo attachment to cytoplasmic motor proteins. Curr. Opin. Cell Biol. *14*, 63–68.

Katsuno, M., Adachi, H., Minamiyama, M., Waza, M., Tokui, K., Banno, H., Suzuki, K., Onoda, Y., Tanaka, F., Doyu, M., et al. (2006). Reversible Disruption of Dynactin 1-Mediated Retrograde Axonal Transport in Polyglutamine-Induced Motor Neuron Degeneration. J. Neurosci. *26*, 12106–12117.

LaMonte, B.H., Wallace, K.E., Holloway, B.A., Shelly, S.S., Ascaño, J., Tokito, M., Van Winkle, T., Howland, D.S., and Holzbaur, E.L.F. (2002). Disruption of Dynein/Dynactin Inhibits Axonal Transport in Motor Neurons Causing Late-Onset Progressive Degeneration. Neuron *34*, 715–727.

Laser-Azogui, A., Kornreich, M., Malka-Gibor, E. and Beck, R., (2015). Neurofilament assembly and function during neuronal development. Curr. Opin. Cell Biol. *32*, 92-101.

Lee, R., Kermani, P., Teng, K.K. and Hempstead, B.L. (2001). Regulation of cell survival by secreted proneurotrophins. Science *294*, 1945-1948.

Lee, R.H. and Mitchell, C.S. (2015). Axonal transport cargo motor count versus average transport velocity: Is fast versus slow transport really single versus multiple motor transport?. J. Theor. Biol. *370*, 9-44.

Lewis, S.E. and Nixon, R.A., (1988). Multiple phosphorylated variants of the high molecular mass subunit of neurofilaments in axons of retinal cell neurons: characterization and evidence for their differential association with stationary and moving neurofilaments. J. Cell Biol. *107*, 2689-2701.

Liot, G., Zala, D., Pla, P., Mottet, G., Piel, M., and Saudou, F. (2013). Mutant Huntingtin alters retrograde transport of TrkB receptors in striatal dendrites. J. Neurosci. *33*, 6298–6309.

Liu, Q.-R., Walther, D., Drgon, T., Polesskaya, O., Lesnick, T.G., Strain, K.J., de Andrade, M., Bower, J.H., Maraganore, D.M., and Uhl, G.R. (2005). Human brain derived neurotrophic factor (BDNF) genes, splicing patterns, and assessments of associations with substance abuse and Parkinson's Disease. Am. J. Med. Genet. Part B: Neuropsychiatric Genetics *134B*, 93–103.

Lu, C. and Mattson, M.P. (2001). Dimethyl sulfoxide suppresses NMDA-and AMPA-induced ion currents and calcium influx and protects against excitotoxic death in hippocampal neurons. Exp. Neurol. *170*, 180-185.

Lu, B., Pang, P.T., and Woo, N.H. (2005). The yin and yang of neurotrophin action. Nature Reviews. Neuroscience *6*, 603–614.

Magrané, J., Hervias, I., Henning, M.S., Damiano, M., Kawamata, H., and Manfredi, G. (2009). Mutant SOD1 in neuronal mitochondria causes toxicity and mitochondrial dynamics abnormalities. Hum. Mol. Genet. *18*, 4552–4564.

Martin, L.J., Liu, Z., Chen, K., Price, A.C., Pan, Y., Swaby, J.A., and Golden, W.C. (2007). Motor neuron degeneration in amyotrophic lateral sclerosis mutant superoxide dismutase-1 transgenic mice: Mechanisms of mitochondriopathy and cell death. J. Comp. Neurol. *500*, 20–46.

Martin, L.J., Gertz, B., Pan, Y., Price, A.C., Molkentin, J.D., and Chang, Q. (2009). The mitochondrial permeability transition pore in motor neurons: Involvement in the pathobiology of ALS mice. Exp. Neurol. *218*, 333–346.

Matthews, V.B., Åström, M.-B., Chan, M.H.S., Bruce, C.R., Krabbe, K.S., Prelovsek, O., Åkerström, T., Yfanti, C., Broholm, C., Mortensen, O.H., et al. (2009). Brain-derived neurotrophic factor is produced by skeletal muscle cells in response to contraction and enhances fat oxidation via activation of AMP-activated protein kinase. Diabetologia *52*, 1409–1418.

Miniou, P., Tiziano, D., Frugier, T., Roblot, N., Le Meur, M. and Melki, J. (1999) Gene targeting restricted to mouse striated muscle lineage. Nucleic Acids Res. *27*, 27-30.

Motil, J., Dubey, M., Chan, W.K.-H., and Shea, T.B. (2007). Inhibition of dynein but not kinesin induces aberrant focal accumulation of neurofilaments within axonal neurites. Brain Res. *1164*, 125–131.

de Moura, M.B., dos Santos, L.S., and Van Houten, B. (2010). Mitochondrial dysfunction in neurodegenerative diseases and cancer. Environ. Mol. Mutagen. *51*, 391–405.

Mowla, S.J., Farhadi, H.F., Pareek, S., Atwal, J.K., Morris, S.J., Seidah, N.G. and Murphy, R.A. (2001). Biosynthesis and post-translational processing of the precursor to brain-derived neurotrophic factor. J. Biol. Chem. *276*, 12660-12666.

Münch, C., Rosenbohm, A., Sperfeld, A.-D., Uttner, I., Reske, S., Krause, B.J., Sedlmeier, R., Meyer, T., Hanemann, C.O., Stumm, G., et al. (2005). Heterozygous R1101K mutation of the DCTN1 gene in a family with ALS and FTD. Ann Neurol. *58*, 777–780.

Nishimune, H., Numata, T., Chen, J., Aoki, Y., Wang, Y., Starr, M.P., Mori, Y. and Stanford, J.A. (2012). Active zone protein Bassoon co-localizes with presynaptic calcium channel, modifies channel function, and recovers from aging related loss by exercise. PLoS One *7*, 38029.

Nguyen, P.V., Marin, L., and Atwood, H.L. (1997). Synaptic Physiology and Mitochondrial Function in Crayfish Tonic and Phasic Motor Neurons. J. Neurophys. *78*, 281–294.

O'Hanlon, G.M., and Lowrie, M.B. (1995). Nerve injury in adult rats causes abnormalities in the motoneuron dendritic field that differ from those seen following neonatal nerve injury. Exp Brain Res *103*, 243–250.

Orr, A.L., Li, S., Wang, C.-E., Li, H., Wang, J., Rong, J., Xu, X., Mastroberardino, P.G., Greenamyre, J.T., and Li, X.-J. (2008). N-Terminal Mutant Huntingtin Associates with Mitochondria and Impairs Mitochondrial Trafficking. J. Neurosci. *28*, 2783–2792.

Ottem, E.N., Bailey, D.J., Jordan, C.L., and Marc Breedlove, S. (2013). With a little help from my friends: Androgens tap BDNF signaling pathways to alter neural circuits. Neuroscience *239*, 124–138.

Palay, S.L. (1956). Synapses in the Central Nervous System. The Journal of Biophysical and Biochemical Cytology *2*, 193–202.

del Peso, L., González-García, M., Page, C., Herrera, R. and Nuñez, G. (1997). Interleukin-3-induced phosphorylation of BAD through the protein kinase Akt. Science *278,* 687-689.

Piccioni, F., Pinton, P., Simeoni, S., Pozzi, P., Fascio, U., Vismara, G., Martini, L., Rizzuto, R., and Poletti, A. (2002). Androgen receptor with elongated polyglutamine tract forms aggregates that alter axonal trafficking and mitochondrial distribution in motor neuronal processes. FASEB J *16*, 1418–1420.

Pineda, J.R., Pardo, R., Zala, D., Yu, H., Humbert, S., and Saudou, F. (2009). Genetic and pharmacological inhibition of calcineurin corrects the BDNF transport defect in Huntington's disease. Mol Brain *2*, 33.

Pomeroy, E.J. (2013). The role of muscle-synthesized brain-derived neurotrophic factor (BDNF) in the health and maintenance of motorneurons. M.S. Northern Michigan University.

Reichardt, L.F. (2006). Neurotrophin-Regulated Signalling Pathways. Philosophical Transactions: Biological Sciences *361*, 1545–1564.

Riccio, A., Ahn, S., Davenport, C.M., Blendy, J.A. and Ginty, D.D. (1999). Mediation by a CREB family transcription factor of NGF-dependent survival of sympathetic neurons. Science *286*, 2358-2361.

Roux, J.-C., Zala, D., Panayotis, N., Borges-Correia, A., Saudou, F., and Villard, L. (2012). Modification of Mecp2 dosage alters axonal transport through the Huntingtin/Hap1 pathway. Neurobiol. Dis. *45*, 786–795.

Rudrabhatla, P., Grant, P., Jaffe, H., Strong, M.J. and Pant, H.C. (2010). Quantitative phosphoproteomic analysis of neuronal intermediate filament proteins (NF-M/H) in Alzheimer's disease by iTRAQ. The FASEB Journal *24*, 4396-4407.

Shah, J.V., Flanagan, L.A., Janmey, P.A., and Leterrier, J.-F. (2000). Bidirectional Translocation of Neurofilaments along Microtubules Mediated in Part by Dynein/Dynactin. Mol. Biol. Cell *11*, 3495–3508.

Shea, T.B., Chan, W.K.H., Kushkuley, J. and Lee, S. (2009). Organizational dynamics, functions, and pathobiological dysfunctions of neurofilaments. Cell Biology of the Axon 160-175. Springer Berlin Heidelberg.

Shi, P., Wei, Y., Zhang, J., Gal, J., and Zhu, H. (2010). Mitochondrial Dysfunction is a Converging Point of Multiple Pathological Pathways in Amyotrophic Lateral Sclerosis. J. Alzheimer's Dis. *20*, 311–324.

Shirendeb, U., Reddy, A.P., Manczak, M., Calkins, M.J., Mao, P., Tagle, D.A., and Reddy, P.H. (2011). Abnormal mitochondrial dynamics, mitochondrial loss and mutant huntingtin oligomers in Huntington's disease: implications for selective neuronal damage. Hum. Mol. Genet. *20*, 1438–1455.

Sternberger, L.A. and Sternberger, N.H. (1983). Monoclonal antibodies distinguish phosphorylated and nonphosphorylated forms of neurofilaments in situ. Proc. Natl. Acad. Sci. *88,* 6126-6130.

Su, B., Wang, X., Zheng, L., Perry, G., Smith, M.A., and Zhu, X. (2010). Abnormal mitochondrial dynamics and neurodegenerative diseases. Biochimica et Biophysica Acta (BBA) - Molecular Basis of Disease *1802*, 135–142.

Su, B., Ji, Y.-S., Sun, X., Liu, X.-H., and Chen, Z.-Y. (2014). Brain-derived Neurotrophic Factor (BDNF)-induced Mitochondrial Motility Arrest and Presynaptic Docking Contribute to BDNF-enhanced Synaptic Transmission. J. Biol. Chem. *289*, 1213–1226.

Sumner, B.E.H., and Watson, W.E. (1971). Retraction and Expansion of the Dendritic Tree of Motor Neurones of Adult Rats induced in vivo. Nature *233*, 273–275.

Taisto, A. E., Madigan, M. R., Dangremond, R. L., and Ottem, E.N. Pathological assessment of neuromuscular junction morphology, myofiber structure, and motorneuron retrograde transport systems in mice missing muscle-synthesized BDNF. Poster session presented at: Society for Neuroscience; 2013 Nov 6-13; San Diego, CA.

Takada, S., Kinugawa, S., Matsushima, S., Mizushima, W., Fukushima, A., Furihata, T., Kadoguchi, T., Yokota, T., Suga, T., Okita, K., et al. (2014). Abstract 12182: Brain-Derived Neurotrophic Factor Maintains Exercise Capacity and Mitochondrial Function in the Skeletal Muscle Through Ampk-Pgc1α Signaling. Circulation *130*, A12182–A12182.

Vos, K.J.D., Chapman, A.L., Tennant, M.E., Manser, C., Tudor, E.L., Lau, K.-F., Brownlees, J., Ackerley, S., Shaw, P.J., McLoughlin, D.M., et al. (2007). Familial amyotrophic lateral sclerosis-linked SOD1 mutants perturb fast axonal transport to reduce axonal mitochondria content. Hum. Mol. Genet. *16*, 2720–2728.

Wagner, O.I., Ascaño, J., Tokito, M., Leterrier, J.-F., Janmey, P.A., and Holzbaur, E.L.F. (2004). The Interaction of Neurofilaments with the Microtubule Motor Cytoplasmic Dynein. Mol. Biol. Cell *15*, 5092–5100.

Waites, C.L., Leal-Ortiz, S.A., Okerlunk, N., Dalke, H., Fejtova, A., Altrock, W.D., Gundelfinger, E.D. and Garner, C.C. (2013). Bassoon and Piccolo maintain synapse integrity by regulating protein ubiquitination and degradation. The EMBO journal *32*, 954-969.

Wang, L., Ho, C., Sun, D., Liem, R.K.H., and Brown, A. (2000). Rapid movement of axonal neurofilaments interrupted by prolonged pauses. Nature Cell Biol. *2*, 137+.

Yang, L.-Y., and Arnold, A.P. (2000a). BDNF regulation of androgen receptor expression in axotomized SNB motoneurons of adult male rats. Brain Res. *852*, 127–139.

Yang, L.-Y., and Arnold, A.P. (2000b). Interaction of BDNF and testosterone in the regulation of adult perineal motoneurons. J. Neurobiol. *44*, 308–319.

Yang, L.Y., Verhovshek, T., and Sengelaub, D.R. (2004). Brain-Derived Neurotrophic Factor and Androgen Interact in the Maintenance of Dendritic Morphology in a Sexually Dimorphic Rat Spinal Nucleus. Endocrinology *145*, 161–168.

Yano, H., Lee, F.S., Kong, H., Chuang, J.-Z., Arevalo, J.C., Perez, P., Sung, C.-H., and Chao, M.V. (2001). Association of Trk Neurotrophin Receptors with Components of the Cytoplasmic Dynein Motor. J. Neurosci. *21*, RC125–RC125.

Yates, D.M., Manser, C., De Vos, K.J., Shaw, C.E., McLoughlin, D.M. and Miller, C.C. (2009). Neurofilament subunit (NFL) head domain phosphorylation regulates axonal transport of neurofilaments. Eur. J. Cell Biol. *88*, 193-202.

Zala, D., Colin, E., Rangone, H., Liot, G., Humbert, S., and Saudou, F. (2008). Phosphorylation of mutant huntingtin at S421 restores anterograde and retrograde transport in neurons. Hum. Mol. Genet. *17*, 3837–3846.

Zheng, Y.L., Li, B.S. and Pant, H.C. (2003). Phosphorylation of the Head Domain of Neurofilament Protein (NF-M) a factor regulating topographic phosphorylation of NF-M tail domain KSP sites in neurons. J. Biol. Chem. *278*, 24026-24032.

APPENDIX A

APPROVAL OF ANIMAL USE BY INSTITUTIONAL ANIMAL CARE AND USE
COMMITTEE

**Application to Use Vertebrate Animals in
Research, Testing or Instruction**

Northern
Michigan
University

Application Number: 241
Date Amended
Application Received:
6/6/2014
Date of Amendment
Approval: 6/27/2014

General Instructions
All parts of this form can be submitted electronically to the Institutional Animal Care and
Use Committee (email: IACUC@nmu.edu), EXCEPT for the signature page. Review of
this application will commence upon receiving the electronic application, but an
application cannot be approved without all required signatures on the hardcopy signature
page (send to IACUC/Graduate Education and Research/401 Cohodas Hall). Please
contact the IACUC chair (email: IACUCChr@nmu.edu) if you have any questions.

Review Dates:
Designated Member Review of applications (appropriate for USDA Use Categories B
and C) will be completed within two weeks after receipt of the electronic application.

Full Committee Review of applications will take place on the third Friday of every
month. Applications for Full Committee Review must be electronically received by the
first Friday of the month. Applications are reviewed by the full IACUC meeting for
USDA Use Categories D and E. A USDA Use Category B or C may be reviewed at a
Full IACUC meeting if requested by an IACUC member. Detailed procedures on the
IACUC review processes are located at the IACUC website.

I. Principal Investigator (Must be a faculty member or Department Head)
Erich N. Ottem, Ph.D.

Co- Investigator
Rebecca Dangremond
Department
Biology
Phone number
906. 227. 1072
Date
02/28/2014

II.   Project/Grant/Course Number and Title (If you will be using external funds, please use the same title as the grant application; if work is for a course, please include the number of the course, title of the course, and a title for the work proposed)

Investigating axonal retrograde transport in motor neurons of muscle-synthesized BDNF deficient mice

Funding Sources (External & Internal) External: NIH/NINDS R15 AREA Grant

Project/Course Start and End Dates March 2014 to March 2017 (three year maximum)

Additional Funding Pending? ☐ Yes   ☒ No

This application is (check one) ☐ New*   ☒ Modification of an application currently approved by the Institutional Animal Care and Use Committee